Pressure drop measurements in microfluidic devices: a review on the accurate quantification of interfacial slip

*Christopher Vega-Sánchez Chiara Neto**

C. Vega-Sánchez, Prof. C. Neto
School of Chemistry and University of Sydney Nano Institute, The University of Sydney, NSW 2006 Australia
Email Address: chiara.neto@sydney.edu.au
C. Vega-Sánchez
School of Electromechanical Engineering, Costa Rica Institute of Technology, Campus Cartago, Costa Rica

Keywords: *microfluidics, interfacial slip, drag reduction, surface contamination*

The correct theoretical definition of boundary conditions of flow underpins all fluid dynamics studies, and is particularly important in situations in which the flow is confined on the nano- and micro-scale. Microfluidic devices are an excellent platform to measure boundary flow conditions, and the pressure drop vs flow rate method is particularly useful in detecting evidence of microscale interfacial slip and drag reduction. This review focuses on the pressure drop method, identifying the main experimental parameters affecting the accuracy and reproducibility of microfluidic experiments of slip, quantifying the magnitude and source of common errors, and providing practical solutions and guidelines. A summary of literature results of interfacial slip obtained with pressure drop measurements in microfluidic devices is also provided, and the slip results are directly compared to expected slip models. This review serves as an introduction for new researchers moving into the field of interfacial slip, and as reminder for established researchers of the need to create highly controlled experimental procedures in order to obtain reproducible and reliable measurements of boundary flow conditions. A direct comparison of accurate experiments with theoretical models is bound to bring about clarity about the mechanisms of slip on smooth and structured surfaces.

1 Introduction

The correct description of boundary conditions for flow underpins all studies in fluid dynamics, and is particularly important when the flow of fluids is confined on the micro- or nano-scale. For over two hundred years, the **no-slip boundary condition**, i.e. the assumption that the relative velocity of the fluid with respect to the wall is zero, was assumed to be valid to describe the dynamics of flow of Newtonian liquids, as it fitted well macroscopic observations (Figure 1a).[1,2] However, around the 1950s the first evidence was found of a reduced resistance to flow for water in hydrophobised capillaries, and was explained with a partial slip boundary condition (Figure 1b).[3,4]

Over the past twenty years, using techniques with nanoscale or microscale resolution, strong experimental evidence of a reduced resistance to liquid flow at non-wettable solid walls has been produced, and this evidence has been interpreted as fluid slip.[1,2] Fluid slip (partial slip) means the tangential velocity of the fluid differs from the that of the solid wall. Fluid slip is quantified by the **slip length**: the ratio of the slip velocity to the shear rate at the wall $b = u_s/\frac{\partial u}{\partial y}$. The slip length is interpreted as the imaginary distance beyond the solid wall at which the linear extrapolation of the fluid velocity vanishes to zero (Figure 1b). Many measurements of the flow of aqueous solutions on smooth hydrophobic surfaces report values of slip length of up to 25 nm, while hydrophilic surfaces display smaller values, down to zero.[1,2] This qualitative relationship between slip length and surface wettability (contact angle) is exemplified in Table 4 and in[5]. Consistently with this trend, much larger, microscale, slip length values are measured when the liquid/solid interfacial area is minimised by design and partially replaced by a liquid/gas interface, such as on superhydrophobic surfaces (Table 5),[6] or by a lubricant/liquid interface, in lubricant-infused surfaces (Table 6).[7] Slip measurements on complex surfaces are described as referring to "apparent slip", i.e. the magnitude of the slip length values is much larger than the length scale of the fluid molecules. Apparent slip is to be distinguished from intrinsic slip (a molecular level slip), a distinction nicely described in previously published reviews.[1,2] Apparent slip is due to fluid flow occurring over a layer of fluid with different viscosity rather than directly on the solid surface (see Figure 1c). In this review we do not delve into the physicochemical mechanisms leading to slip, but given that an

"effective slip" can be measured, we focus on approaches to increase the reproducibility and accuracy of its measurement.

The concept of **effective slip** is considered to be most useful to describe most experiments and for practical applications. Effective slip implies that the slip is quantify over the length scale of the measuring apparatus, which might include smaller areas in which different boundary conditions apply (e.g. areas containing nanobubbles or patterns of different wettability, on which different extent of slip may occur). Effective slip should be understood as the equivalent slip required on a smooth uniform solid surface that would produce the same flow conditions far away from the surface. The occurrence of slip implies a significantly reduced hydrodynamic resistance for the fluid to flow, an effect that becomes relevant at microscopic scales, and that may lead to important gains in energy efficiency. As a result, in the last decades research efforts have been put in developing analytical [8–18] and numerical models [16,19–22] aimed at predicting the effective slip on walls and optimize the surface characteristics (e.g. topography and lubricant selection) to maximize the fluid slip. Several highly-regarded reviews on slip on smooth and structured surfaces exist. [1,2,5,6,23–25]

As presented in section 7 of this review, many studies report experimental measurements of slip but, in general, it is found that the reported data is scattered and, in many cases, slip length values of orders of magnitude larger than the theoretical models have been measured. As slip is a desirable practical property and its study is imperative for the fundamental understanding of flow, it is important to be able to measure it accurately and reproducibly. Therefore, this review focuses on the assessment of the pressure drop versus flow rate method used to measure the slip boundary condition for flow in the laminar regime. Based on our own work [26] and previous works found in the literature, best practice procedures are identified, guidelines for the proper use of the method provided and strategies to improve its accuracy recommended.

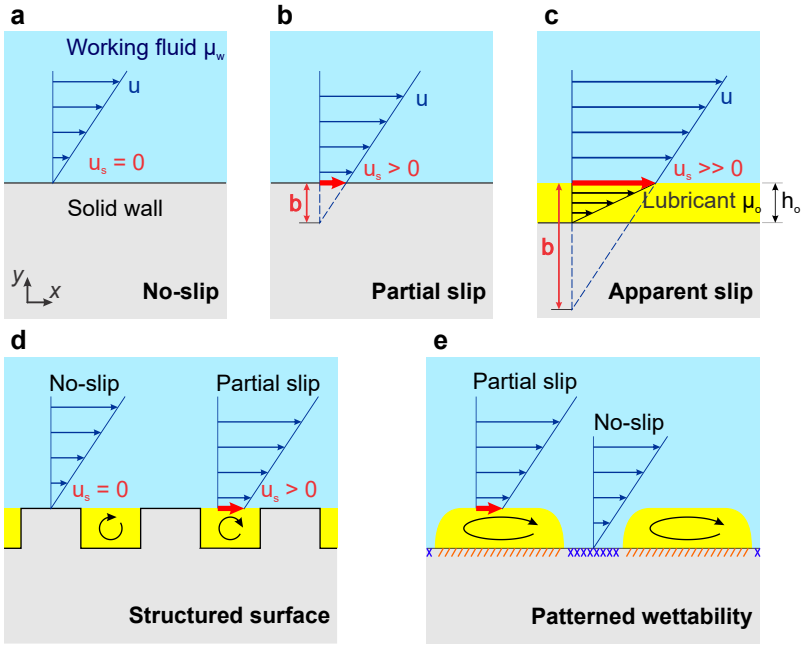

Figure 1: Wall boundary conditions. (a) No-slip, (b) partial slip, (c) apparent slip produced by a lubricating film, (d) apparent slip produced by a structured lubricant-infused surface and (e) patterned wettability leading to a lubricant being retained on a surface. For all the cases, the solid substrate is represented in gray, the working fluid in blue and the lubricant in yellow.

2 Slip at complex walls

The occurrence of slip on complex walls, such as a solid wall infused with a lubricating fluid of height h_o, produces an **apparent slip** as depicted in Figure 1c. For a given lubricant film thickness h_o, if the

viscosity of the lubricating fluid μ_o is lower than that of the working fluid μ_w, the change in the shear rate across the fluids can produce a large interfacial velocity. Consequently, assuming the continuity of the velocity field and the shear stress at the interface, the apparent slip length can be computed as $b = \frac{\mu_w}{\mu_o} h_o$.[27] Although the scenario of a continuous lubricant layer is ideal for enhancing fluid slip of the working fluid, it has clear issues regarding its practicality. Firstly, achieving a continuous and stable lubricant film is difficult. For thick lubricant films, instabilities of the lubricant-fluid interface appear due to interfacial tension between the immiscible fluids which tends to deform the interface; on the other hand, for thin lubricant films, the disjoining pressure produced by the van der Waals interactions could also cause the lubricant to dewet from the solid substrate.[28,29] If the lubricant is a gas layer, the continuous layer scenario is not thermodynamically stable when located between a liquid and a solid wall.[30] Secondly, assuming that the lubricant can be stabilized under flow conditions, the system will require a continuous pumping of lubricant along with the working fluid in order to maintain a lubricant layer and avoid depletion due to its flow.

To overcome these challenges, the lubricating layer can be stabilized by trapping within a micro- and nano-structure. This can be achieved either by using a structured non-wettable surface that creates spots for contact line pinning (Figure 1d) or by using a surface with patterned wettability[31] (Figure 1e). In practice, structured non-wettable surfaces, called lubricant-infused surfaces, are used, and superhydrophobic surfaces can be considered one such special surface in which the lubricant is air. Disregarding the way in which the lubricant is stabilized, the slip induced by pockets of lubricant is always smaller than the one that could be achieved by a continuous lubricant layer of the same thickness.[2] In isolated lubricant pockets, the entrapped lubricant is forced to recirculate within a confined space (Figure 1d and e), reducing its apparent slip.[32,33] Additionally, the creation of the three phase contact line implies that now the working fluid is in direct contact with the solid wall which intrinsically displays a small (nanoscale) slip. Nonetheless, lubricant-infused surfaces offer a good compromise between achieving large slip and producing robust surfaces. As lubricant-infused surfaces are characterised by locally-dependent boundary conditions, the concept of effective slip appropriately describes the overall slip measured on these surfaces.

3 Techniques for quantifying fluid slip

The quantification of the slip length in experiments has been achieved by direct methods or indirect methods, which were thoroughly reviewed in the past.[1,2,24] Here for brevity we mention some of these methods. Direct methods rely on the precise determination of the velocity profile near the wall and, consequently, provide information of the slip condition locally. These methods create maps of the slip length over a specific region of the surface and help us to understand how the surface chemistry or topography affect the fluid slip locally. For example, they provide information on how the transition from a no-slip to a partial slip condition occurs in structured surfaces containing gas pockets (Figure 1d). Techniques such as particle image velocimetry, fluorescent recovery after photobleaching and fluorescence correlation spectroscopy are used for this purpose.[1] Direct methods are excellent in extracting spatially-dependent information about slip, which enables the comparison of experimental observations with theoretical models. Nonetheless, their ability to map extensive areas is limited due to the complexity of the experimental setup.

Indirect methods aim to quantify the effective slip on a surface. These methods normally rely on the measurement of macroscopic quantities such a pressure, flow rate and net forces acting on bodies [1,6]. Accordingly, they provide information about the effect of the surface on the overall behaviour of the interfacial flow. Among these techniques are pressure drop vs flow rate, hydrodynamic drainage forces between two surfaces (surface force apparatus [34–37] and colloid probe atomic force microscopy [38–40]), shear stress measurement (typically using a rheometer) [41,42] and sedimentation of particles [43,44]. With the exception of the hydrodynamic drainage force measurements, these techniques normally require simpler experimental setups in comparison with direct methods. As a result, they have been used extensively to evaluate the slip performance of a wide range of surfaces. The apparent ease of use of indirect meth-

ods popular belies subtleties which, if overlooked, may lead to the incorrect estimate of the effective slip length. In this review the focus is on the parameters and procedures that must be taken into consideration when using the pressure drop vs flow rate method for quantifying slip under laminar flow conditions.

4 Fundamental background of the pressure drop vs flow rate method

4.1 Pressure drop and estimation of the effective slip length

Consider an incompressible fluid of density ρ and viscosity μ flowing through a horizontal circular pipe of constant radius R (Figure 2a). The energy balance equation between point 1 and 2 can be written as follows:[45]

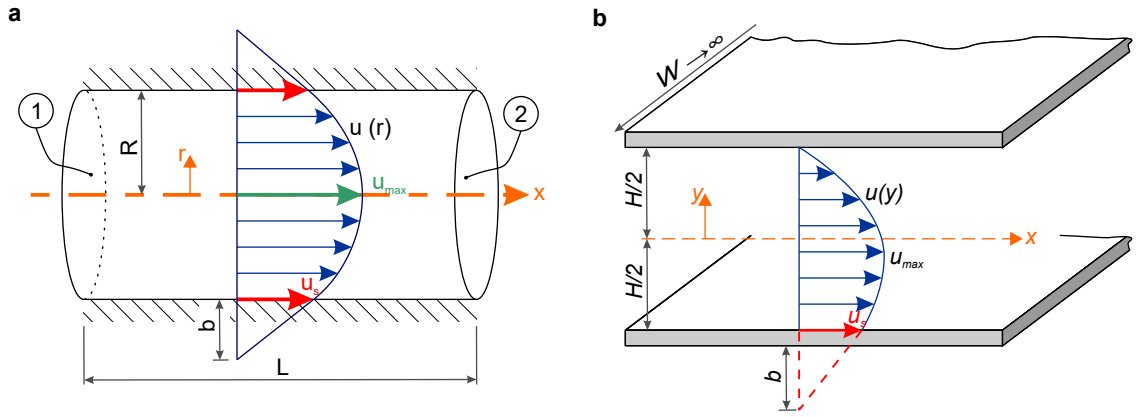

Figure 2: Flow through (a) a circular pipe and (b) two infinite parallel plates.

$$\left[\alpha_1 \frac{V_1^2}{2g} + z_1 + \frac{p_1}{\rho g}\right]_{inlet} - \left[\alpha_2 \frac{V_2^2}{2g} + z_2 + \frac{p_2}{\rho g}\right]_{outlet} = h_f, \tag{1}$$

where h_f represents the energy lost by the fluid as it is transported through the pipe, α is the kinetic energy correction factor ($\alpha \approx 2$ for laminar flow), $V = Q/A$ is the average velocity over the cross-sectional area A for an average flow rate Q, z the height given from an arbitrary reference system, p the static pressure, and g the gravity constant. If the cross-sectional area is constant and the pipe is horizontal, then $V_1 = V_2$ and $z_1 = z_2$, from which we conclude that the energy loss can be quantified through a measurement of the pressure drop along the pipe:

$$h_f = \frac{p_1 - p_2}{\rho g} = \frac{\Delta p}{\rho g}. \tag{2}$$

From Figure 2a, for the case of a steady laminar pressure-driven flow, assuming axisymmetric flow and no tangential velocity, the pressure drop can be estimated as:[45]

$$\Delta p = \frac{8\mu L Q}{\pi R^4}\left(\frac{1}{1 + 4b/R}\right) \tag{3}$$

where L is the pipe length.
From the above equation it can be observed that the pressure drop is inversely proportional to the slip length b, i.e. the pressure drop is maximum for a no-slip boundary condition ($b = 0$) and is minimum (zero) for a large (infinite) slip length. Eq. 2 dictates that the energy loss while transporting the fluid is directly proportional to the pressure drop, therefore, inversely proportional to the slip length as well. This implies that the amount of energy loss in the fluid can be adjusted by changing the wall properties and tuning the slip length b.

Equations 2 and 3 provide the basis for the experimental estimation of the slip length through the so-called pressure drop vs flow rate method. Given that Δp, μ, Q, L and R can be measured experimentally, then the effective slip length b can be computed readily.
In a similar manner, the analysis can be made for a fully developed laminar flow between two infinite parallel plates, one of which displays a partial slip condition (Figure 2b). In this partial slip case, the pressure drop can be estimated as[45]:

$$\Delta p = \frac{4\mu L Q}{H^3}\left(\frac{1}{3}+\frac{b}{b+H}\right)^{-1} \tag{4}$$

where H is the separation distance between the plates and Q is the flow rate per unit width. This equation is widely used for the estimation of the effective slip of surfaces when using channels with rectangular cross section with high aspect ratio W/H, where W is width of the channel. For $W/H > 20$, the wall effects become negligible and this simplification can be made.[45,46]

4.2 Slip length or drag reduction?

Using the pressure drop vs flow rate method, the effective slip length and the drag reduction factor can be estimated. These two quantities are directly linked but they have different meaning. Although they are used interchangeably in the literature, this practice could be lead to misinterpretation. In general, the slip length is a property of the surface itself (associated only to the fluid shear rate imposed upon the wall, i.e. proportional to the fluid viscosity) and, therefore, it is not expected to change with the scale of the system (some exceptions are presented in[47] and discussed in[10]). On the other hand, the drag reduction is a comparative estimation of the amount of energy saved by transporting the fluid through a system with slip against the same system containing zero slip. Therefore, drag reduction depends on system size. Using the pressure drop vs flow rate method, the drag reduction factor can be estimated in two ways:

1. Fixing the pressure drop along the channel/pipe and measuring the enhancement of the flow rate through slip:

$$DR_Q = \frac{Q_{exp}-Q_{ns}}{Q_{ns}} \tag{5}$$

   where Q_{ns} is the average flow rate across the channel cross section under a no-slip condition at the wall, and Q_{exp} the experimentally measured flow rate. This comparison is made for systems under exactly the same pressure drop and with exactly the same geometry and size.

2. Fixing the flow rate through the channel/pipe and measuring the reduction in the pressure drop:

$$DR_P = \frac{\Delta p_{ns}-\Delta p_{exp}}{\Delta p_{ns}} \tag{6}$$

   where Δp_{ns} and Δp_{exp} are the pressure drop given by a no-slip condition and the experimentally measured pressure drop, respectively, for systems under exactly the same flow rate and exactly the same geometry and size.

Q_{ns} or Δp_{ns} can be derived theoretically from equations 3 or 4 taking $b = 0$. However, for the flow along rectangular channels, Eq. 4 relies on the assumption that $W/H >> 1$. More generally, Q_{ns} or Δp_{ns} can be derived from the friction factor equation:[45]

$$\Delta p_{ns} = \frac{f}{\mathrm{Re}}\frac{\rho V^2 L}{2D_h}, \tag{7}$$

where Re is the Reynolds number, D_h the hydraulic diameter of the channel and the friction factor f can be estimated for each specific experiment according to the channel aspect ratio W/H.[45]

As mentioned above, the drag reduction factor is influenced by the system size. For example, for a pressure-driven laminar flow through a circular pipe (Eq. 3), the drag reduction factor DR_P can be estimated as:

$$DR_P = \frac{1}{1 + R/4b} \tag{8}$$

Given a fixed value of slip length b, the smaller the system (smaller R), the larger the drag reduction factor would be. In the same way, for rectangular cross-sectional channels with high aspect ratio W/H the drag reduction is given by:

$$DR_P = 3/(4 + H/b). \tag{9}$$

Although the drag reduction factor provides information about the energy saving given by a particular surface, it is given only for a specific system size and geometry. On the contrary, the slip length value is, in general, a surface property, irrespective of the system size in which it is used. Therefore, different surfaces should be compared by comparing slip length values and not drag reduction factors.
An important implication of this is that substantial energy savings are only possible when the slip length is of the same order of magnitude as the characteristic length of the system. For example, for the two systems presented in Figure 2, a 10% drag reduction would be achieved when b is around 3% of the characteristic length of the system (i.e. R or H). This implies that for large systems, such as oil pipelines or ships, macroscopic slip length values would be needed in order to accomplish a significant reduction of drag. Therefore, achieving large drag reduction in large scale systems only by surface modification is a challenge, but it is extremely beneficial for the manipulation of fluids at smaller scales.

5 Measurements of pressure drop vs flow rate

5.1 Experimental apparata

A variety of experimental apparata have been used to quantify the effective slip using the pressure drop vs flow rate method. Figure 3 and Table 1 present a selection of experimental apparata and measurement methods employed in literature studies, and highlight that different approaches are commonly used. Experimentally, there are two different ways to carry out a pressure drop vs flow rate experiment, which we will call "comparative method" and "absolute method". In the comparative method, two systems are directly compared, one containing no-slip walls and the other one with surfaces designed to allow for a partial slip. This approach normally relies on the assumption that both systems are exact copies of each other (including fluid viscosity and exact channel size), with the only difference being the testing surface. Under this assumption, equations 5 to 9 can be used to extract the effective slip length without the need to know the fluid properties (mainly viscosity μ) and pipe/channel length L. Another advantage of this method is that it does not require measuring simultaneously the pressure drop and the flow rate, given the fact that Eq. 5 and Eq. 6 only depend on the estimation of a single variable: Q or Δp. Therefore, when this method is used, one of the variables must be fixed, either the flow rate or the pressure drop, and the second must be measured. Figure 3a-b show a schematic of the setups. This experimental approach is low cost as fewer sensors are needed but has the drawback that it is hard to guarantee that the fluid properties remain constant between experiments and it is complex to ensure that the systems geometries and sizes are identical. Shirtcliffe et al.[48] propose a way to avoid these issues. They used the comparative method 1 showed in Figure 3a and measured the pressure drop along copper tubes at a fixed flow rate to compare structured versus as-received tubes. Their setup, however, consists of a single syringe pump connected to four parallel testing ports on which four types of tubes were randomly switched between positions to minimize systematic sources of error (see Figure 3d). In this way They avoided experimental errors related to comparing data from separate experiments on individual surfaces. In addition, they also carried out the experiment at different flow rates to test the slip effect of the structured surfaces at higher pressures. Kim and Hawng[49] used the comparative method 2 shown in Figure 3b. They fixed the pressure drop along a superhydrophobic tube (shown in red and mark with

number 11 in Figure 3e) and quantified the mass transport enhancement as a consequence of the liquid slip at the wall. The setup uses a syringe (10) driven by a constant pressure of compressed air (2). The balance (7) is used to quantify the mass flow rate over time. Some additional examples of the use of these comparative methods are shown in Schnell[4] and Lee[50].
Between the two comparative methods shown in Figure 3a-b, fixing the flow rate and measuring pressure drop (comparative method 1 in Figure 3a) is a more reliable way to carry out these experiments, because fixing the pressure along the channel (comparative method 2 in Figure 3b) is experimentally challenging. This is normally done by applying a certain pressure head at the supply reservoir connected at the inlet and, consequently, any change in the connection line between the reservoir and the inlet port, or a change in the outlet port, changes the pressure applied at inlet of the microchannel, therefore affecting Δp.
The absolute method quantifies the slip length using the setup shown in Figure 3c. In this case both the pressure drop and the flow rate must be measured accurately, and used to derive the slip length directly from Eq. 4, given that the remaining variables are known (μ, L and H). Experimentally, this approach is more complex because all the variables must be measured accurately and simultaneously, but has the advantage that it does not rely on a comparison between different systems. In addition, it provides higher confidence in the reported value of the effective slip length because all the experimental variables are monitored during the experiment. A good example of the setup used in this method is presented by Kim and Hidrovo[51] in Figure 3f. The setup was used to study the friction behaviour of rectangular channels containing superhydrophobic walls with transverse trenches. They quantified the pressure drop using a differential pressure transducer connected near the inlet and outlet of the channel and simultaneously measured the mass transport along the system by collecting and weighting the water using a balance. They also controlled and monitored the temperature of the system to account for variations in the fluid viscosity.

5.2 Methods to pump liquids

Irrespective of the setup used to carry out experiments, the liquid is pumped in a microfluidic device by applying pressure (e.g. pressure provided by a fluid column due to gravity or by a pressurized reservoir), by a recirculation pump, by a peristaltic pump or by a syringe pump. Figure 4 shows schematics of these methods. Pressure-driven mechanisms provide more stable flow (flow rate and pressure) compared with peristaltic or syringe pumps, and are therefore more likely to provide high quality data, as shown in Figure 4a, in which data from real experiments is presented. The fluctuations in the flow rate produced by the syringe pump cause large fluctuations in the pressure drop along the microfluidic channel. Syringe pumps are limited by the volume of the syringe and, in general, the use of larger syringes produces larger fluctuations in the flow rate. On the contrary, pressure-driven systems can use larger fluid supply reservoirs and therefore are able to operate for longer times (up to days). Examples of compressed air and water column pressure-driven systems can be seen in Figure 3e and f, respectively. Table 1 is a summary of the pumping mechanisms used in previous studies.

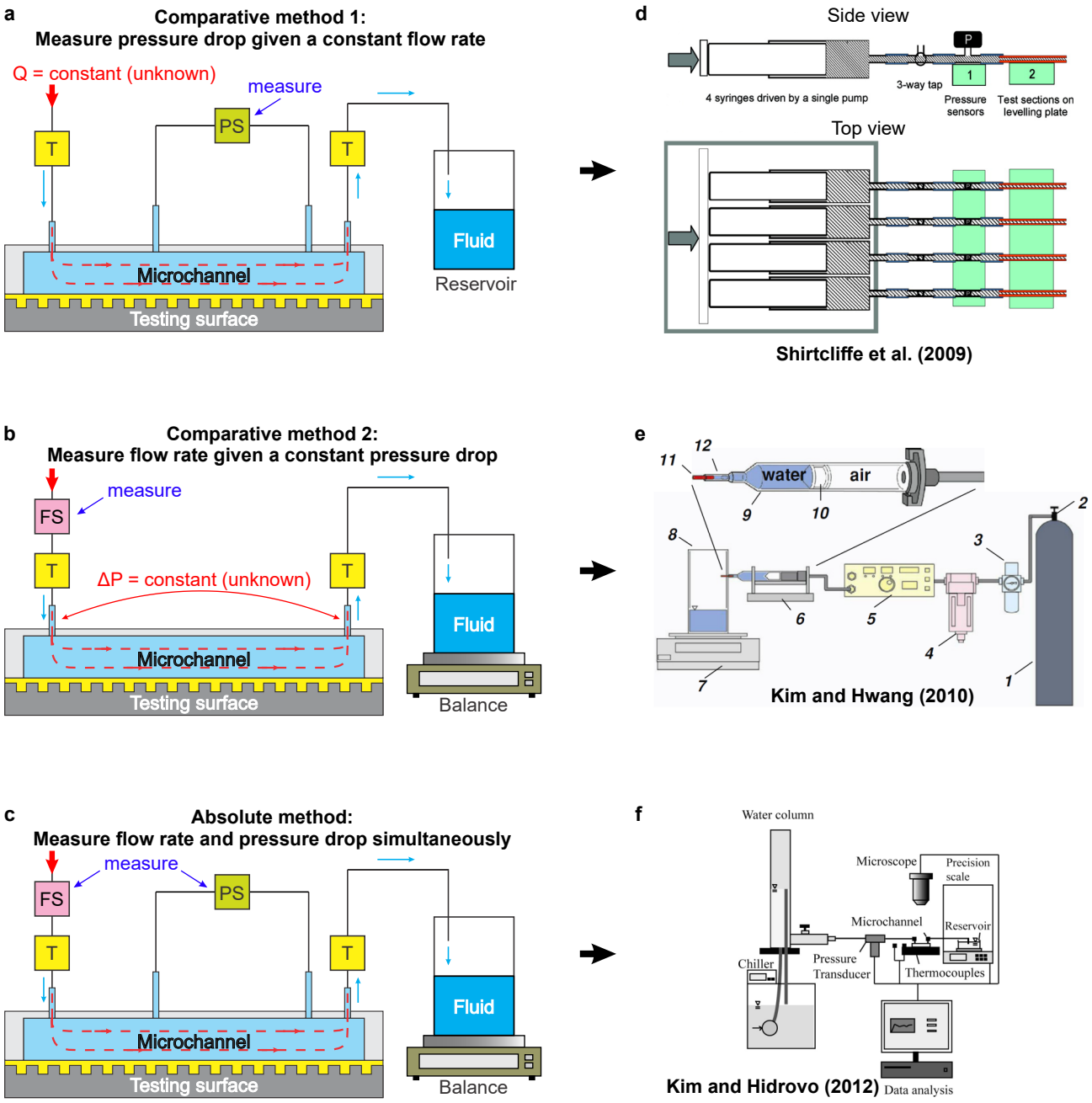

Figure 3: Experimental setups used for carrying out the pressure drop vs flow rate method to quantify the effective slip length of surfaces. FS: flow sensor, PS: differential pressure sensor, T: temperature sensor. (a) Setup used to measure the pressure drop given that the flow rate is fixed (although unknown) and is kept fixed irrespective of the conditions of the system. (b) Setup used to measure the enhancement of the flow rate through the system given that the pressure drop along the channel is kept constant (although it is unknown) irrespective of the conditions of the system. (c) Setup in which the flow rate and the pressure drop are measured simultaneously. Examples of each configuration are shown in (d) adapted with permission from Shirtcliffe et al.[48] Copyright 2009 American Chemical Society, (e) adapted with permission of Kim and Hwang (2010)[49] ©IOP Publishing. All rights reserved. (f) Reprinted from Kim and Hidrovo (2012),[51] with the permission of AIP Publishing.

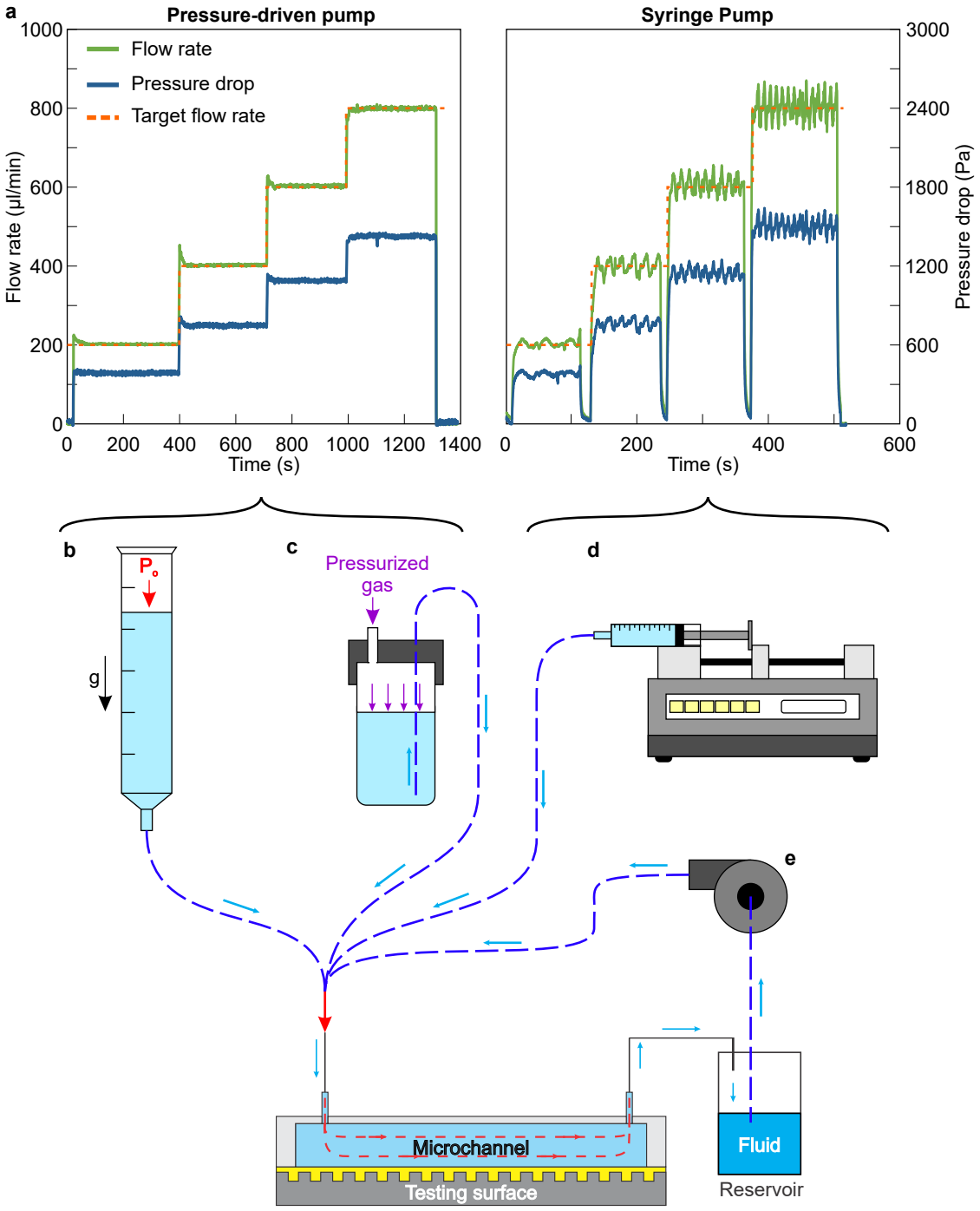

Figure 4: Experimental data and mechanisms to drive fluid through a microfluidic channel. (a) Flow rate and pressure drop curves as a function of time for the same microchannel using a pressure-driven system (left hand side, OB1 Pressure Controller Mk3, Elveflow) and a syringe pump (right hand side, GenieTouch, Kent Scientific). The flow rate and pressure drop were measured continuously over time using a flow sensor MFS3 (Elveflow) and a pressure transducer PX459-10WDWU5V (Omega), respectively. Schematic microfluidic setup in which the fluid flow is driven by (b) a water column drives by gravity, (c) pressure using pressurized gas, (d) a syringe pump, (e) a recirculation pump (e.g. centrifugal pump or peristaltic pump).

When employing a pressure-driven system which uses pressurized air to drive the fluid, the concentration of dissolved air in the water could increase substantially. According with Henry's law, the amount of dissolved gas in a liquid is proportional to its partial pressure. This could become problematic when driving fluids through small and long microchannels because the static pressure needed to pump the fluid could be significantly high. High concentrations of gas in the working fluid could promote the nucle-

ation of bubbles on the testing substrate, specially on rough hydrophobic ones. From a practical point of view, large bubbles impede the collection of stable data and need to be excluded by degassing the liquid. Nanoscale or microscale bubbles can be tolerated and are likely to increase the interfacial slip measured, given the low viscosity of the gas.[26] This is an issue that could be avoided using a syringe pump.

5.3 Methods to measure liquid flow rate and pressure drop

The flow rate can be measured using different techniques. Commonly, an analytical or precision balance is used to quantify the mass flow rate over time, as shown in Figure 3b-c and e-f. The use of balances offers some challenges: firstly, sudden changes in the flow rate cannot be estimated and the estimation of flow rate is only accurate over long periods. Secondly, the evaporation of the working fluid in the open or semi-open reservoir becomes significant when the mass flow rate is small and must be considered in order to reduce the experimental error.[51] And finally, the correct estimation of the volumetric flow rate relies on the proper estimation of the fluid density, which depends on the temperature. Other techniques of measurement of flow rate rely on the measurement of the displacement of an advancing or receding interface. For example, by recording over time the rise of a meniscus in a calibrated capillary tube. The interface can be tracked using a camera or using a laser-distance meter (see[52]). Particle image velocimetry is also used to estimate the velocity of the fluid. A more complex but highly accurate way to estimate the flow rate is by measuring the time-of-flight of an ionic sample between two electrodes positioned at a known distance (see[53]). More simply, flow sensors can be installed in line with the tubing at the inlet or outlet of the microfluidic channel. These sensors normally operate under the principle of thermal time-of-flight. Table 1 summarizes the most commonly used methods to quantify flow rate in previous studies.

It is best practice to measure the pressure drop at two points in the middle section along the microfluidic channel to guarantee that the flow is fully developed and avoid disturbances produced by the inlet and outlet ports. Ideally, two ports should be dedicated only for pressure drop measurements. This, however, could be challenging for small channels and capillaries. Therefore, another approach is to measure the pressure drop between the inlet and outlet but in this case the inlet and outlet losses should be considered.[54] In practice, the pressure drop can be measured using a single differential pressure sensor, two gauge sensors or one gauge sensor (assuming that the outlet port is always at a constant and known pressure, e.g. atmospheric pressure, as shown in Figure 3d), as detailed in Table 1. A single differential pressure transducer is shown in Figure 3a and c connected to pressure-dedicated ports. Pressure drop can be also quantified using a pressure gauge manometer or a standard column manometer. However, column manometers should be extremely clean to avoid pressure disturbances due to the pinning of the contact line of the meniscus and the Laplace pressure of the free interface (see section below on Surface cleanliness and preparation).

When assessing the amount of sensors to use for measuring the pressure drop, the best criterion for selection is to estimate the error propagation of each configuration and select the one that produces less experimental uncertainty. For example, using two gauge sensors to measure the pressure drop will produce an uncertainty of $\sigma(\Delta p) = \sqrt{\sigma_1^2 + \sigma_2^2}$, where $\sigma(\Delta p)$ is the uncertainty in the estimation of the pressure drop, and σ_1 and σ_2 are the uncertainties of each individual sensor. The error propagation is also discussed later in this article. Disregarding the selected configuration to measure the pressure drop, the most important characteristics of the pressure sensor for this application are its resolution (minimum measurable quantity) and its accuracy. When measuring the pressure drop, special care must be taken in reducing bubbles trapped in the connection tubing between the port and the sensor. Trapped bubbles change the pressure drop due to the Laplace pressure of the liquid-air interface.

Table 1: Selection of microfluidic apparata used in previous studies of interfacial slip.

Authors	Setup type [1]	Fluid	Pump	Pressure drop measurement	Flow rate measurement
Smooth substrates					
Schnell (1956) [4]	b	water	Pressure-driven (column and pressurized nitrogen)	–[2]	Mass flow rate (precision balance)
Churaev (1984) [55]	c	water, mercury, CCL4 and benzene	Pressure-driven (pressurized nitrogen)	–[2]	Meniscus tracking (microscopy)
Mala (1999) [54]	c	water	Precision pump (Ruska Instruments)	Pressure transducer (1x gauge)	In-line flow sensor and mass flow rate (precision balance)
Cheng (2002) [56]	c	water, silicone oil, hexane, hexadecane, decane	Syringe pump	Pressure transducer (1x gauge)	Meniscus tracking (microscopy)
Choi (2003) [57]	c	water	Pressure-driven (pressurized nitrogen)	Pressure transducer (2x gauge)	Meniscus tracking (laser-distance meter)
Structured hydrophobic substrates					
Watanabe (1999) [47]	c	water and 20-30% glycerol water	Centrifuge and pressure driven (compressed air)	Pressure transducer (1x diff.)	Mass flow rate (precision balance) and hot wire anemometer
Ou (2004) [58]	c	water	Syringe pump	Manometer (water)	–[2]
Choi (2006) [59]	c	water	–[2]	–[2]	Mass flow rate (precision balance)
Shirtcliffe (2009) [48]	a	water and 50% water glycerol	Syringe pump	Pressure transducer (4x gauge)	–[2]
Jung (2009) [60]	c	water and air	Syringe pump	Pressure transducer (1x diff.)	–[2]
Kim (2010) [49]	b	water	Pressure-driven (pressurized air)	–[2]	Mass flow rate (precision balance)
Kim (2012) [51]	c	water	Pressure-driven (column)	Pressure transducer (1x diff.)	Mass flow rate accounting for evaporation (precision balance)
Kashaninejad (2012) [61]	c	water	Pressure-driven (column)	–[2]	Meniscus tracking (microscopy)
Lee (2014) [50]	b	water	Pressure-driven (pressurized air)	–[2]	Meniscus tracking (high-speed camera)
Song (2014) [46]	c	water	Syringe pump	Manometer (water)	–[2]
Structured liquid-infused substrates					
Kim (2016) [62]	c	water and glycerol mixtures	Syringe pump	Manometer[3]	–[2]
Lee (2019) [63]	c	water[3]	Syringe pump	Pressure transducer (1x diff.)	–[2]

[1] The letters refer to labels used in Figure 3.
[2] Not reported or unclear.
[3] Inferred from figures.

5.4 Small deviations in the experimental measurements lead to large errors in the effective slip length

Systematic deviations or inaccuracies in the measurements of the experimental variables could cause significant deviations in the estimate of the effective slip length or the drag reduction factor. In this Section the effect of systematic experimental deviations is explored assuming they are caused by a lack of accuracy e.g. not well-calibrated sensors or non-constant ambient temperature.
Given the complexity and number of variables needed to quantify the effective slip on surfaces (Eq. 3 and Eq. 4), the analysis is carried out numerically for a representative case. Consider the flow of water through a microfluidic channel of rectangular cross section of height $H = 100$ µm and width $W = 2$ mm (high aspect ratio $W/H = 20$). The distance between the pressure ports is $L = 50$ mm and the channel is sufficiently long to avoid parasitic effects produced by the inlet and outlet ports in the measurement of the pressure drop Δp.[45,54] These values were chosen to represent typical dimensions of microfluidic channels employed in this kind of experiments. Let us assume that the bottom wall of the channel is a surface with a known effective slip length $b = 3$ µm, and flow rate Q, pressure drop Δp and temperature T (used to determine the viscosity of the water) are measured using the setup shown in Figure 3c. Using Eq. 4 the effective slip length could be determined experimentally, given that all the remaining variables are known.
Figure 5a shows the deviation in the estimate of the effective slip length induced by the inaccurate quantification of each variable, assuming that each variable acts independently. For example, the deviation induced by an inaccuracy in the estimation of L is presented for the case in which the rest of the variables (Q, T, W, Δp and H) were measured with full accuracy.

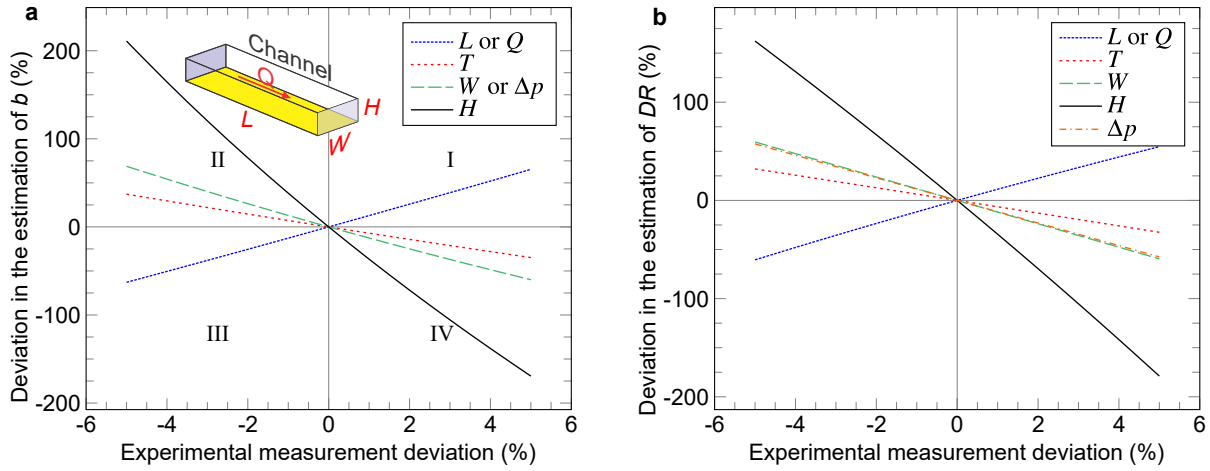

Figure 5: Deviation in the estimate of the (a) effective slip length or (b) drag reduction factor as function of deviation in each experimental measurement. Each curve represents the deviation induced by a single variable, assuming that the remaining measurements were affected by no error. The values presented correspond to the case of flow of water at $T = 25$°C through a rectangular channel of $H \times W \times L = 0.1 \times 2 \times 50$ mm^3. The temperature T is used to estimate the viscosity of the water through the Vogel equation $\mu = e^{(-3.7188+578.919/(135.604+T))}$, where T is in °C.

The abscissa in Figure 5a is plotted for experimental deviations between -5% and +5%, while the ordinate axis reaches values as high as +200%. This observation is indicative of the high accuracy required in these experiments to correctly estimate b. Negative measurement deviations are underestimates of the experimental quantity, while positive ones are overestimates of the experimental variable. The plot is divided in four quadrants (I, II, III and IV): in quadrant I the overestimate of the experimental quantity leads to an overestimate of the effective slip length. For example, a 2% overestimation of L or Q induces a 26% overestimate of b (i.e. instead of measuring $b = 3$ µm, the result would be $b = 3.8$ µm). In II, the underestimate of the experimental measurement results in the overestimate of b. In III and IV the slip length is underestimated given the underestimation or overestimation of the experimental measurement, respectively.

The largest deviation in the estimate of b is produced by deviations in channel height H. A 2% underestimate of H causes a 78% overestimate of b (i.e. instead of measuring $b = 3$ µm, the result would be $b = 5.3$ µm). Similarly, a 2% underestimation of T or Δp generates a 15% or 26% overestimate of b, respectively.
A similar analysis is carried out for the estimate of the drag reduction factor DR in Figure 5b. For this particular analysis, equations 6 and 7 were used under the assumption that the testing surface produces a $DR = 8\%$. Again, the most influential value in the determination of the correct value of DR is the channel height H: 3% underestimation will translate to a 100% of overestimation in DR (i.e. instead of measuring $DR = 8\%$, the result would be 16%).
These considerations are a good indication of the expected influence of the experimental variables on the correct determination of b and DR for systems of similar length scales. Small deviations in the quantification of experimental variables indisputably produce large deviations in the estimation of the slip length, and therefore measurements of interfacial slip require extreme care in maximising experimental accuracy.

5.5 Design of microfluidic devices

Microfluidic devices are normally made using a layer-by-layer approach in which different layers of materials are assembled to create the microchannels, valves and ports. Micromachining techniques, such as additive, subtractive and pattern transfer techniques, are used for making these layers; photolithography and etching processes are at the core of these techniques and are widely used to create microstructures for microfluidics[64]. Simple microfluidic devices commonly consist of two layers, one of which contains the microfluidic channels, while the other acts as an enclosing layer, as shown in Figure 6a. This is the approach used for building microfluidic devices made of PDMS and glass, an extensively used technique for microfluidics. The two layers can be joined permanently (e.g. fully bonded, Figure 6b) or can be held together by fasteners or clamps (e.g. separable or modular devices, Figure 6c). Both approaches have been used for quantifying effective slip on surfaces. Some examples are presented in Figures 6d-f.
Fully bonded devices offer the advantage of being geometrically well-defined and suffer less deformation because the bonding process normally is done chemically or electrostatically. However, a new device is required each time a different surface needs to be tested and not all substrates can be bonded (e.g. PTFE and lubricant-infused surfaces). On the other hand, modular devices offer more versatility in exchanging the testing substrate without the need of making a new device, but are prone to deformation due to the clamping force.
Rigidity and geometry are key aspects in designing microfluidic devices for quantification of the effective slip length. As shown in Eq. 3 and 4, the correct estimate of b depends critically on the high accuracy measurement of the geometric dimensions of the microchannel: R and L (for circular pipes) or H, W and L (for rectangular channels), with R or H being the most critical lengths, as presented in Figure 5. These dimensions must be measured carefully, and they must remain unchanged during the experiment. Therefore, the microfluidic device must be rigid enough to ensure that under the applied hydrostatic pressure to drive the fluid, the microchannel does not deform significantly. Additional care must be taken when closing or clamping modular devices aimed to interchange the testing substrate. An excessive clamping force could lead to deformation of the channel, changing its shape and size.
Table 2 shows the materials used to fabricate microfluidic devices presented in selected previous studies. Due to their lower tendency to deform, rigid materials such as silicon, aluminum, glass and rigid polymers (e.g. PMMA) should be used to build microfluidic devices for slip measurements. Devices shown in Figures 6e-f are excellent examples of the use of these materials. Although PDMS is widely used in microfluidics, it is well-known to deform easily under pressure. Figure 7 shows the maximum normalized deformation $\bar{\delta} = \delta/H$ produced by static pressure applied on the inner walls of a channel of rectangular cross section and original height H, for different material properties. The deformation for the rectangular channel was estimated from a finite element method model implemented in COMSOL Multiphysics. For the circular pipe the deformation was estimated assuming a thin-wall pipe using the equation $\delta/R = pR/bE$, where p is the inner static pressure, R the inner radius of the pipe, t the wall thick-

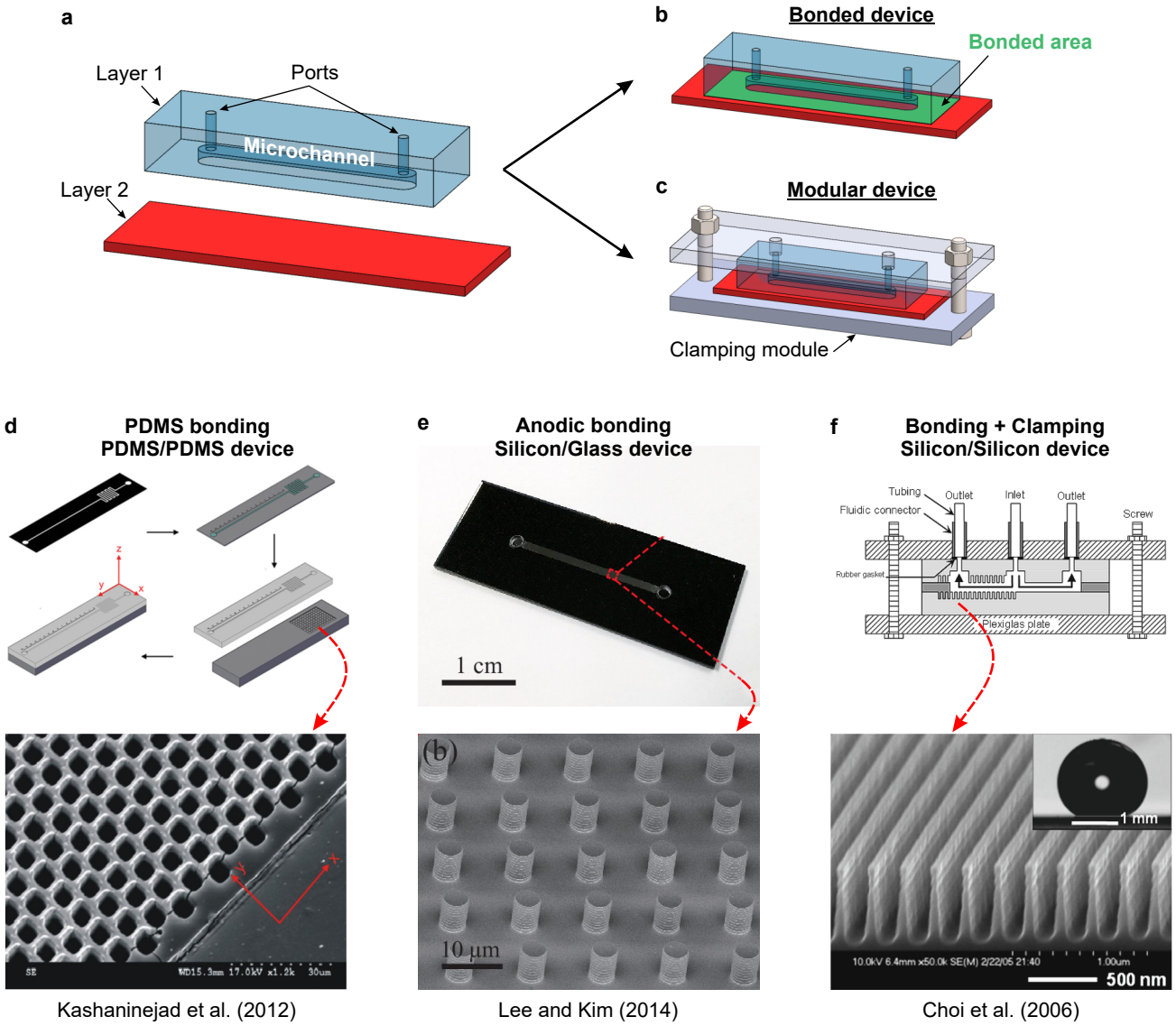

Figure 6: (a) Key elements of a microfluidic devices: a top surface containing the microfluidic channels, and bottom surface. (b) Fully bonded device. (c) Separable modular device built using a clamping module. Examples of commonly used approaches to build microfluidic devices: (d) device consisting of two layers of PDMS bonded with a thin layer of PDMS, one layer contains the microfluidic channel geometry and the other one is decorated with holes; (e) device built by anodic bonding of a glass wafer and a silicon substrate decorated with posts; (f) silicon/silicon device containing nanoridges in both walls and bonded through a photoresist layer and then reinforced by mechanical clamping. Panels (d-f) are adapted from Kashaninejad et al. (2012),[61] Lee and Kim (2014),[50] and Choi et al. (2006),[59], respectively, with the permission of AIP Publishing.

ness (assumed as $t = R/10$) and E the Young's modulus of the material. Among the materials plotted in Figure 7, PDMS shows the highest maximum deformation corresponding to values of 7 and 4% for the rectangular and circular channel, respectively. However, the increase in the cross section total area is larger for the circular pipe, approximately 8% against a 5% for the rectangular channel. The numerical simulations also show that reinforcement on the top and bottom walls (e.i. assuming that the external walls are fixed) does not help in reducing the deformation of the PDMS channel given that it is easily compressible. The normalized maximum deformation for the reinforced case reached 6.6% (versus 6.8% for the case without reinforcement), this is shown as red star in Figure 7. This result shows that reinforcement will be only effective in mitigating excessive deformation if the channel material is rigid enough to avoid excessive compression under the applied static pressure. Also, it is expected that larger deformations will occur in rectangular channels of higher aspect ratios W/H.

These increments in the cross section induced by applied pressure can lead to overestimating the effective slip length of the testing surfaces. For a given flow rate, the expanded cross section causes a lower hydrodynamic resistance along the channel and, therefore, a lower pressure drop. If neglected, this effect could be misinterpreted as a reduction in the pressure drop due to fluid slip on the testing surface. In a similar way, for a fixed pressure drop along the channel, the increased cross sectional area will lead to an enhancement of the flow rate, resulting in the same misinterpretation of the experimental data. Fortunately, rigid materials strongly reduce this issue. For the same conditions presented above, the rectangular microchannel made with PMMA only has an increase in the cross sectional area of 0.003%, while for glass, aluminum and silicon the deformation is five orders of magnitude smaller than for PDMS, or virtually zero.

An additional aspect to consider when designing microfluidic devices is visual access to the microfluidic channel, to detect the formation of bubbles or other flow disturbances. One or both of the building layers should be transparent e.g. glass or PMMA. Thin glass slides and thin silicon wafers are flexible and deform easily under static pressure, even when bonded to rigid substrates. Choi et al.[59] address this issue by reinforcing the bonded device with a clamping mechanism, as shown in Figure 6f. For devices built completely out of opaque materials, the conditions of flow can be inferred from the experimental variables such as pressure drop and flow rate along the device but this require close attention and expertise.

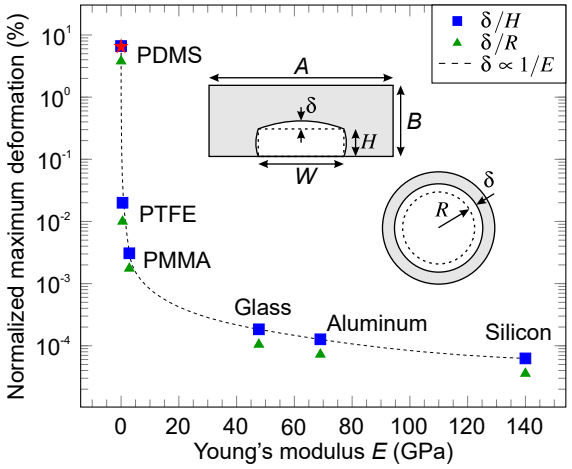

Figure 7: Normalized maximum deformation of the cross section of a rectangular and circular microchannel as a function of the Young's modulus of the material E. The deformation for the rectangular channel was estimated from a finite element method model implemented in COMSOL Multiphysics for a channel of $H = 100$ µm and $W/H = 20$, $A = 20$ mm and $B = 10$ mm, which are common in microfluidic devices. The internal static pressure was assumed to be $p = 5000$ Pa which approximately corresponds to the expected pressure drop along the rectangular channel of length $L = 50$ mm for a water flow rate of $Q = 1\ \mathrm{mL\,min^{-1}}$. The blue squares correspond to the case in which only the bottom wall of the geometry is fixed, while the red star shows the result for the case in which the top and bottom walls are fixed (e.g. reinforced by a more rigid material).

5.6 Definition of the reference plane

As discussed before, the channel height H is the most significant experimental variable affecting the correct estimation of the effective slip length. Two factors are key in the proper determination of H: first, the reference plane from which H is measured, and second, the change of size due to the assembly process of the device.
The definition of the reference plane is important in cases for which the measured effective slip length b or the channel height H are of the same order of magnitude as the characteristic surface roughness (or surface topography). As depicted in Figure 8a, smooth surfaces are the closest to an "ideal" flat surface, free of defects, and characterized by low values of roughness parameters (peak-to-valley roughness R_z, average roughness R_a and root mean squared roughness R_{rms}). Common examples of smooth surfaces are mica, silicon wafers, and thin films over silicon wafer (e.g. grafted layers), for which typical R_{rms} is smaller than 0.3 nm. In structured surfaces a structure has been introduced explicitly to alter the surface topography. Structured surfaces can be further categorized as patterned (e.g. micropillars, grooves, holes or cavities) or randomly structured (e.g. wrinkles, sanded or etched surfaces), as show in Figure 8b-c and Figure 10a.

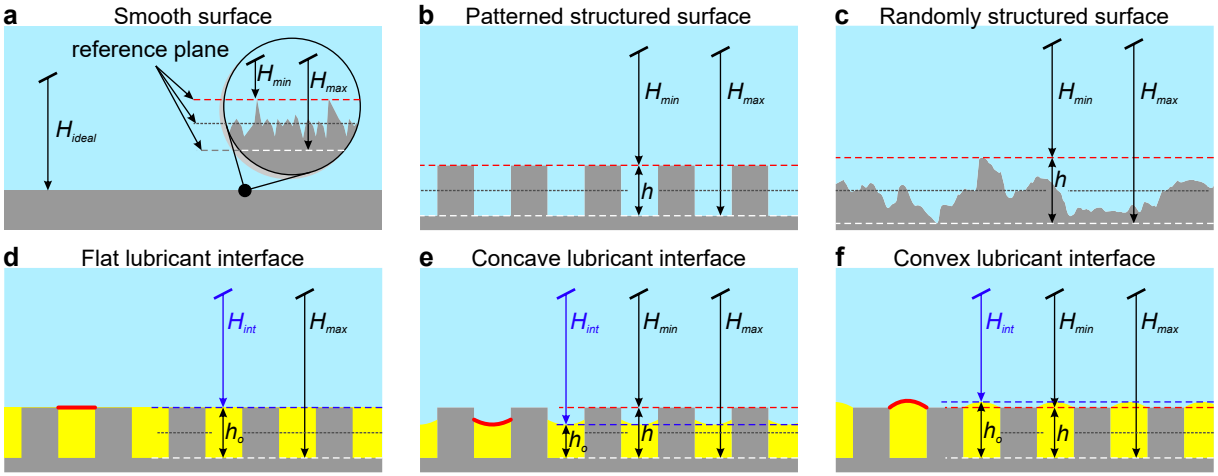

Figure 8: Definition of the reference plane for different solid substrates, such as (a) smooth, (b) patterned structured, (c) randomly structured surfaces, (d) an ideal flat interface containing a lubricant (yellow), (e) a concave lubricant interface pinned below the corner of the surface topography, and (f) a convex lubricant interface pinned at the corner of the surface topography. The reference plane could be chosen anywhere between the bottom (white dashed line) and the top (red dashed line) of the surface features.

Table 2: Selection of materials used for building microfluidic apparata and testing substrates in the literature.

Authors	Device type	Channel type	Channel material	Testing substrate material	Substrate position	Channel dimensions		
						H or R (µm)	W (µm)	L (mm)
Schnell (1956) [4]	Connection of capillary	Capillary tube	Pyrex	Pyrex	Capillary inner wall	R 240 to 800		1000
Churaev (1984) [55]	Connection of capillary	Capillary tube	Quartz	Quartz	Capillary inner wall	R 0.31 to 7.2		57.1 - 97.6
Mala (1999) [54]	Connection of capillary	Capillary tube	Stainless steel and fused silica	Stainless steel and fused silica	Capillary inner wall	R 25 to 127		28.5 - 88.0[1]
Cheng (2002) [56]	Bonded (photoresist)	Rectangular channel	Thin cover glass and photoresist	Photoresist	All walls	0.04 to 2.7	<20[2]	0.1 to 0.9
Choi (2003) [57]	Bonded (anodic)	Rectangular channel	Silicon and Pyrex	Silicon	All walls	1 and 2	500	9
Watanabe (1999) [47]	Connection by fittings	Pipe	Acrylic resin	Fluorine alkane with silica	Pipe inner wall	R 3000 to 6000		475
Ou (2004) [58]	Modular (clamped)	Rectangular channel	Plastic and glass	Silicon	Bottom wall	76 to 254	$20 \times H$	50
Choi (2006) [59]	Bonded (photoresist)	Rectangular channel	Silicon and photoresist	Silicon	Top and bottom walls	2 to 12	400 and 1000	4
Shirtcliffe (2009) [48]	Connection of capillary	Capillary tube	Copper	Copper	Capillary inner wall	R 438		110 - 84
Jung (2009) [60]	Bonded (glue)	Rectangular channel	Plastic	Epoxy	Top and bottom walls	700	2500	60
Kim (2010) [49]	Connection of capillary	Capillary tube	Polyamide coated with PTFE	PTFE nanofibers	Capillary inner wall	R 500		10
Kim (2012) [51]	Bonded (O_2-plasma)	Trapezoidal channel	PDMS	PDMS	Side walls	120	∼100	18.5
Kashaninejad (2012) [61]	Bonded (PDMS)	Rectangular channel	PDMS	PDMS	Bottom wall	17.9	220	41.25
Lee (2014) [50]	Bonded (anodic)	Rectangular channel	Glass	Silicon	Bottom wall	30	1000	20
Song (2014) [46]	Modular (clamped)	Rectangular channel	PDMS reinforced with acrylic	Sanded PTFE	Bottom wall	137	3400	45
Kim (2016) [62]	Modular (clamped)	Rectangular channel	PDMS reinforced with acrylic	PDMS and sanded PTFE	Bottom wall	150	3500	45
Lee (2019) [63]	–[3]	Rectangular channel	PDMS	PVA	Bottom wall	600	4000	70

[1] The pressure drop was estimated from the difference in the pressure drop between two capillaries of different length. Check the reference for details.
[2] Adjusted to keep the flow rate within measurable range.
[3] Not reported or unclear.

The reference plane can be defined relative to the solid substrate geometry or relative to the fluid/fluid interface. In the first case, it can be placed anywhere between the top (H_{max}, red dashed line in Figure 8) and the bottom (H_{min}, white dashed line) of the substrate roughness or structure. In the second case, it can be placed wherever the interface is located (H_{int}, blue dashed line). For a lubricant-infused surface, the apparent slip equation is normally defined from the lubricant-fluid interface (see equation $b = (\mu_w/\mu_o)h_o$ above). This seems to be consistent with the observation that in infused surfaces the fluid interface is assumed to be located and pinned exactly at the top of the surface topography (see Figure 8d).

Other important aspects affecting the effective slip length are the shape and location of the lubricant-fluid interface.[12,18,20,37] In general, theoretical models are derived for the cases in which the interface is assumed to be flat and pinned exactly at the top of the surface topography.[10,11,14] Indeed, it is common practice in the literature, although not often correct, to assume that the lubricant height h_o is equal to the topography height h.[42,62] Although it is experimentally complex to describe the interface shape and location, the lubricant-fluid interfaces is normally not flat and can be located at any position within the structure given the pinning of the three-phase contact line (see Figure 8e-f).[65] This situation can give rise to important discrepancies between theoretical models and experimentally measured slip length values.

The location of the interface within the surface topography is determined by the local pinning of the three-phase contact line and the volume of lubricant in the system. As shown in Figure 8e, the surface topography could be only partially filled with lubricant, which could be the result of an incomplete infusion of the lubricant during the preparation of the surface or due to lubricant depletion caused by a number of factors, including the shear stress imposed by the working fluid[33,62] or dissolution of the gas into the liquid.[66–68] A reduced amount of lubricant increases the roughness of the surface on which the external fluid flows, which in turn reduces the effective slip. Indeed, Richardson demonstrated that even in the extreme and ideal case in which the solid walls display a zero-shear-stress condition, the roughness produced by the exposed solid surface could result in an overall no-slip condition at the wall.[69,70] On the other hand, if the lubricant is slightly in excess (e.g the lubricant-fluid interface protrudes above the top of the solid structures), the effective slip can be enhanced greatly, given that the fluid does not need to decelerate to meet the no-slip condition a the solid wall.[16] In a counterintuitive manner, lubricant depletion could also increase the overall height of the channel. For example, in surfaces containing pillars, the lubricant depletion could create new passages for the fluid to flow in between the pillars, increasing the height of the channel from H_{min} to H_{int} as shown in Figure 8e. In these conditions, the flow rate could be enhanced or the pressure drop along the channel reduced. Our recent computational fluid dynamics simulation study explores in detail these effects for lubricant-infused surfaces.[71].

The shape of the lubricant-fluid interface also affects the effective slip. Steinberger et al. reported that the protrusion of gas pockets on a superhydrophobic surface can cause a reduction in the effective slip, even in the case in which the interface is pinned at the top of the solid structure.[37] They predicted through a numerical model that it is possible for a bubble mattress to display a negative slip length (e.i. the no-slip plane is located within the channel, above the tops of the solid substrate). Using a two-phase lattice Boltzmann simulation, Hyväluoma and Harting showed the dependence of the slip length with respect the curvature of the gas bubbles.[20,21] They found that the maximum slip length given by a structured surface with attached gas bubbles is achieved when the gas-liquid interface slightly protrudes from the cavity (as shown in Figure 8f). However, strongly protruding interfaces produce negative slip lengths. These results were later reproduced by the analytical model developed by Davis and Lauga,[12] and Asmolov et al.[18] Interestingly, these studies suggest that slightly convex and protruding fluid interfaces, and not perfectly flat ones, are expected to increase the slip while virtually reducing the overall height of the channel. This counterintuitive behavior was later explained by Haase et al.[72]

Finally, in some cases, the positioning to the reference plane can change the interpretation of the obtained data: defining the plane at the bottom of the surface topography ($H = H_{max}$ in Figure 8) could be interpreted as a surface not enhancing slip, while positioning the plane at the top of the topography could lead to the opposite conclusion. This topic has been addressed in detail in[15].

5.7 Measurement of channel height

The height of a microfluidic channel H should be quantified once the device has been fully coupled with the testing surface and not prior to assembly. The process of joining the microfluidic channel to the substrate could change the final height H (see Figure 9). In the case that the channel is bonded (Figure 6b), the height could be affected by the use of adhesive or sealing materials (Figure 9b). Although the use of an adhesive layer is normally not an issue for most microfluidic applications, here a 1 µm-thick adhesive layer could translate into a ∼40% error in the estimate of b or DR (Figure 5). On the other hand, when using a modular device (Figure 6c) the clamping force could cause indentation of the microchannel into soft substrates (e.g. polymeric substrates) which could lead to a substantial reduction of H (Figure 9c).
Occasionally, the device is assembled and then the channels walls are treated to change their properties, for example, by flowing solutions that react to the wall to create absorbed layers or structures. This technique is widely used to coat capillary tubes or small pipes to alter their interaction with the external fluid.[4,47,48,55] In these cases, the channel height and width are both decreased (Figure 9d) and these corrections are difficult to establish ex situ. Finally, the combination of these effects is possible; for example, when using an auxiliary clamping device to join the parts, it is common practice to use a sealant film to avoid leaks. Hence, the proper determination of the channel dimensions is probably the most complex task to address in these experiments.

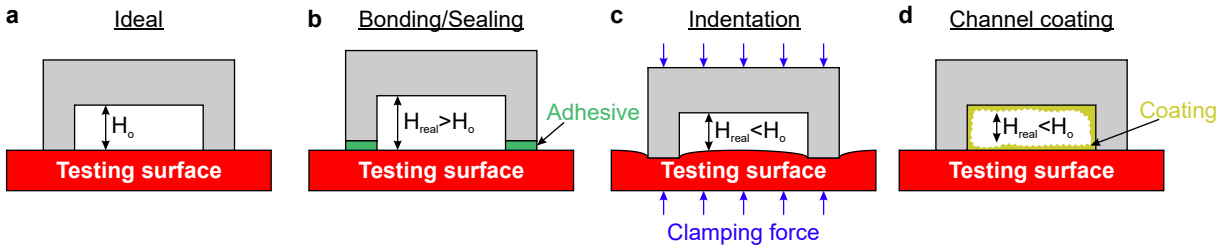

Figure 9: Effect of assembly method on the final channel height H. (a) Ideal condition in which the original channel height H_o remains unchanged after assembly. (b) Adhesive or sealant layers increase the channel height. (c) Compression causes indentation of the substrate, reducing the channel height. (d) Flowing of an adsorbing solution may lead to the decrease in channel height.

Finding ways to directly measure the channel height once the device is assembled is difficult but crucial. Estimating or simply approximating the channel height induces a large error in the quantification of the slip length and therefore should be avoided. In Table 3, some approaches used in previous studies to overcome this challenge are presented.
Here we propose some alternatives to accurately measure the channel height:

1. For fully bonded devices the pressure drop vs flow rate experiment can be carried out and, then the device can be diced to get direct access to the cross section of the channel. Ideally, several cross section should be measured. This is a well-establish technique and it is highly reliable if done properly. This approach is only valid if the channel does not deform under the applied static pressure.

2. For modular devices dicing is not an option given that the main purpose of clamping the device is to use it multiple times. The authors have solved this problem by, first, carrying out the experiment and, then, without opening the device, filling the channel with PDMS (Sylgard 184, in a ratio of 5:1) to create an exact replica of the microfluidic channel.[26] The curing of the PDMS is done a room temperature to avoid thermal expansion of the microfluidic device which could affect the final size of the replica. Once cured, the device is opened and the replica is measured accurately using profilometry, or cut in sections and measured directly by optical microscopy.

3. In principle with a design as the one used in[57], it should be possible to measure channel height with interferometry in situ.

Table 3: Selection of techniques used to measure the channel characteristic length H or R in microfluidic devices.

Authors	Channel characteristic length H or R (µm)	Uncertainty	Technique used to measure H or R
Schnell (1956) [4]	R 240 to 800	–[1]	Capillaries were filled with mercury and the mass and volume of mercury were used to estimate the radius.
Churaev (1984) [55]	R 0.31 to 7.2	1% to 14% [2]	1) Radius was fitted based on the flow rate for hydrophilic capillaries. 2) Radius was estimated using the capillary pressure of liquids (benzene or CCl4) completely wetting the capillaries.
Mala (1999) [54]	R 25 to 127	1% to 4%	–[1]
Cheng (2002) [56]	0.04 to 2.7	∼5%	1) Estimated from photoresist manufacturer's specification; 2) Inferred from the conductance of a channel filled with an electrolyte (dilute nitric acid).
Choi (2003) [57]	1 and 2	∼7%	Measured before bonding using profilometer and then corrected using two fitting models. Error between measurement and fitting was found to be ∼7%.
Watanabe (1999) [47]	R 3000 to 6000	–[1]	Pipe radius was estimated as an average between inlet and outlet radius of the pipe.
Ou (2004) [58]	76 to 254	–[1]	–[1]
Choi (2006) [59]	2 to 12	∼5%	Measured before bonding using profilometer and then fitted from the flow rate data obtained from smooth-surface channels with the assumption of no-slip at the walls. Error between measurement and fitting was found to be ∼5%.
Shirtcliffe et al. (2009) [48]	R 438	–[1]	–[1]
Jung (2009) [60]	700	–[1]	–[1]
Kim (2010) [49]	R 500	–[1]	–[1]
Kim (2012) [51]	120	∼2% [2]	Measured before bonding using microscopy (M = 40×, NA = 0.60)
Kashaninejad (2012) [61]	17.9	–[1]	–[1]
Lee (2014) [50]	30	–[1]	–[1]
Song (2014) [46]	137	–[1]	Measured after the channel was sealed using microscopy and later confirmed by fitting flow rate data obtained from smooth Teflon surface with the assumption of no-slip.
Kim (2016) [62]	150	–[1]	–[1]
Lee (2019) [63]	600	–[1]	–[1]

[1] Not reported or unclear.
[2] Estimated from data presented in the article.

5.8 Measurement of liquid viscosity and temperature

As shown in Figure 5 (red dashed line), temperature significantly influences the correct estimation of the effective slip length and drag reduction factor by affecting fluid viscosity and density. For the analyzed case, 1 °C of deviation in the measurement of the temperature induces a 26% error in the quantification of b. For water, according with the Vogel equation the viscosity is given by:

$$\mu(T) = e^{-3.7188+\frac{578.919}{135.604+T}}, \tag{10}$$

where T is the temperature in °C. An increase in the water temperature of 1 °C causes a decrease of approx. 2% in the viscosity. Given the high sensitivity of the viscosity to changes in temperature, the pressure drop vs flow rate experiment must be carried out under controlled and monitored temperature. Several studies in the literature report slip length values measured at "room temperature", which suggests that temperature was not monitored and could fluctuate substantially, causing large variations in the estimated values of b and making the experiments irreproducible.

Microfluidic devices are great heat exchangers due to the large area-to-volume ratio of the microfluidic channel. Therefore, the fluid temperature should be measured in situ and continuously, preferably at the outlet or directly on the microfluidic device. The temperature of the fluid at the reservoirs could differ significantly from the fluid temperature at the inlet or outlet of the device and, therefore, should not be measured.

Although water is used in most of the experiments on slip, the use of more viscous fluids is also required when evaluating the effect of the viscosity ratio μ_w/μ_o on the slip length. Glycerol or sucrose aqueous mixtures are often employed. Given that these fluids absorb water from the ambient easily and viscosity specified by manufacturers is not known with sufficient accuracy, the viscosity vs temperature curve must be experimentally determined using an accurate rheometer.

5.9 Surface cleanliness and preparation

As with any experiment in which surfaces play an important role, all sources of potential contamination should be minimized when measuring slip in microfluidic device. The accumulation of impurities or surfactants at self-contained lubricant-liquid interfaces (e.g. interfaces that are isolated and confined) can rigidify the interface which could potentially lead to its immobilization and suppress its capacity to transfer momentum. This effect has been shown to produced a no-slip condition in superhydrophobic spheres,[73] however, it is not well-studied in liquid-infused surfaces yet.[25]

Below is a list of the ten most important considerations to keep in mind when undertaking surface science experiments that require a high level of cleanliness:

1. Use only high purity water and solvents. When performing experiments that require aqueous solutions, use only high purity water, such as as Milli-Q, with conductivity $\approx 18.2\ \mathrm{M}\Omega cm^{-1}$. Milli-Q water should be collected in clean glass vessels shortly before conducting each experiment, and unused water should be exchanged at least daily. With organic solvents, use only high purity analytical grade solvents. Filtering with fine (200 nm) filters should be considered to remove dust particles.

2. Use only glassware and accessories that have been cleaned thoroughly. Glassware and accessories which will come in contact with the apparatus should be cleaned immediately before being used, and rinsed copiously. Dirty glassware can be detected with the simple rinse test: allow water to drain out of glassware; if water droplets are left behind, the glass is not clean (a continuous thin films should form on clean glass).

3. Develop a cleaning protocol for samples. The sources of contamination even in a relatively clean lab are multiple, and constant care should be used to minimise them. For samples, an appropriate protocol should be developed that eliminates the source of contamination but does not destroy the chemical or topographical details desired on the surface. Surfaces and accessories should be handled only with clean powder-free gloves or clean tweezers and stored in clean Petri dishes. Prepare samples in a laminar flow cabinet to reduce dust contamination. Low cost and portable versions of laminar flow cabinets are available commercially as well as the more expensive permanent ones. A standard cleaning protocol

for silicon wafers and other robust surfaces is the following: sonicate in ultrapure ethanol for 1 minute and blow dry under a pure nitrogen stream; repeat the same with acetone. Plasma treat the surface for 1 minute (commercial units such as the ones sold by Harrick are sufficient for this purpose). In addition, a CO_2 snow gun can be used to remove dust particles (the sample should be heated to avoid condensation during the treatment, see point 4).

4. Do not allow wet surfaces to dry in air. Any liquid droplet placed on a surface, and especially high surface tension liquids such as water, are a ready receptacle of dust and hydrophobic contaminants in the air. When the droplets evaporate, they deposit these contaminants on the surface, accelerating the fouling problem. Liquids should be blown dry off the surface using a stream of high purity nitrogen (usually house nitrogen piped through Chemistry buildings is not of sufficient purity).

5. Use only accessories made of glass or teflon. Most syringes, containers, and other lab accessories made of plastic release trace amounts of oligomers when immersed on solution. The use of plastic implements should be avoided when conducting experiments that require extreme cleanliness. Teflon tweezers have the added advantage of being softer that metal ones, so they reduce the formation of debris particles when handling brittle samples such as silicon wafers.

6. Store samples and accessories in clean conditions. Sample storage should be carefully considered: e.g. avoid storing samples in the same cabinet as other samples containing low surface tension (super-spreading) oils such as silicone oils. Clean containers should be arranged for even short term storage of samples and accessories during and before experiments, to reduce dust and cross-contamination. Recently cleaned glass Petri dishes can have this function.

7. If a cleaning protocol has been developed and works, do not alter it or skimp on steps. Individual surface science laboratories develop cleaning protocols that are appropriate for their experiments. Once these protocols are proven to be effective, they should be adhered to in detail, as often changing even one step of a protocol can have unpredictable effects, and the source of the contamination can be impossible to establish. For example, in one occasion the source of contamination could not be established. Eventually it was found that the experiment was compromised by the fact that Milli-Q water was being dispensed from the unit prior to the reading on the unit reaching the minimum conductivity of 18.2 $M\Omega cm^{-1}$. The problem with experiments immediately disappeared when this issue was addressed.

8. Always question the purity and cleanliness of commercial and synthesised chemicals and surfaces. In most surface science experiments, additional cleaning of chemicals is required, whether they be commercially purchased or synthesised in house. The use of surface tension, NMR spectra and other high accuracy analytical techniques can indicate the need for elimination of dust, oligomers, surfactants, and other contaminants.

9. Consider explicitly the potential effect of dissolved impurities and gases in your results. In many surface science experiments, as well as in other disciplines, the effect of trace impurities, including air, can dominate the observed effects. Egregious examples are in the spurious discovery of "polywater" in the 1960s (finally attributed to contaminated water[74]) and the measurement of inexplicably long-range attractive forces between hydrophobic forces (eventually attributed to the nucleation of bubbles between hydrophobic surfaces).[75] The possibility that impurities are skewing the results should always be considered and tests performed to verify the hypothesis.

10. Consider explicitly the effect of temperature, humidity, light exposure, sample history and other environmental factors on your experimental protocol. In best practice experimental design, detailed records of environmental factors should be kept, as often it is not until later in the investigation that the key factors become apparent. As some of these environmental factors are harder to control than others, it is sensible to advance in steps from the simplest to the most difficult factor to control and test. The easiest factor to control is the temperature, which needs to be measured in situ within the measurement apparatus. As discussed above, temperature affects most physical properties of liquids such as viscosity, density, and surface tension, and these effects can be significant in microfluidic measurements. The second parameter of importance is environmental humidity, which can be adjusted by using controlled gas flows or saturated solutions of salts in enclosed chambers. Environmental humidity affects a wide range of surface measurements and reactions, from tribological charging of surfaces to adhesion between parti-

cles, from the phase separation of water soluble polymers, to the apparent nanoscale topography of adsorbates onto surfaces, to the outcome of surface silanisation reactions on silicon waters. All surfaces exposed to atmospheric pressure are coated with sub-nanometer water films, which can be eliminated by heating to temperatures above 65 °C for many hours.[76]

5.10 Validation of experimental setup

Validation is the method to prove that the experimental setup does what it is intended to do. This is a fundamental step, must be done frequently and must be fully documented. The validation of the process must consist in testing the accuracy, precision, range of measurement and robustness of the setup. It is good practice to check the characteristics of individual sensors prior to interconnecting them in the final setup. For the pressure drop vs flow rate method, it would be ideal to test the flow sensor, the differential pressure sensor, the temperature sensors and the instruments used to determine the channel dimensions. Each sensor must be tested, at least, to the full range of the expected operation while carrying the pressure drop vs flow rate experiment. Ideally, only sensors with calibration certificate should be used, however, this normally implies a high cost.
Robustness is often overlooked in flow experiments. Microfluidic sensors are affected by vibration, movement and/or ambient temperature. Therefore, tubing and accessories should be fixed and any disturbance avoided while carrying out the measurements. The position of tubing can cause changes in the static pressure and losses in the system, which translate in variability of the experimental measurements. The validation of the setup could be done by constructing the pressure drop vs flow rate curve following Eq. 7 for a well-known smooth material in which the slip is expected to be zero. When water is used, silicon wafers and smooth glass surfaces are excellent candidates for this purpose. In general, it is recommended to use as a validation substrate one that has high affinity with the working fluid to avoid possible trapping of gas bubbles. The validation must be done for different flow rates and different temperature values and, if possible, using different microfluidic devices.

5.11 Error propagation and uncertainty in the estimation of the slip length

Every experimental measurement is associated with an uncertainty. Given that the slip length is a subtle effect, and often nanoscale, it is particularly important to evaluate the experimental uncertainty in slip measurements. Given that several experimental variables influence the pressure drop vs flow rate experiment to determine the slip length, the propagation of all these errors defines the uncertainty with which the slip length is computed. The overall uncertainty must be estimated taking into account the individual uncertainty associated with each experimental variable as follows (based on Eq. 7):

$$\sigma_b^2 = \left(\frac{\partial b}{\partial W}\right)^2 \sigma_W^2 + \left(\frac{\partial b}{\partial H}\right)^2 \sigma_H^2 + \left(\frac{\partial b}{\partial L}\right)^2 \sigma_L^2 + \left(\frac{\partial b}{\partial T}\right)^2 \sigma_T^2 + \left(\frac{\partial b}{\partial Q}\right)^2 \sigma_Q^2 + \left(\frac{\partial b}{\partial \Delta p}\right)^2 \sigma_{\Delta p}^2, \tag{11}$$

where σ_b is the uncertainty in the estimation of the slip length b and σ_i is the uncertainty in the experimental measurement of the i variable (e.g. σ_H is the uncertainty of the experimental measurement of the channel height H) and $\frac{\partial b}{\partial i}$ is obtained by differentiating b with respect to $i-$variable.[77] Normally, each of these uncertainties σ is considered as one standard deviation of the sample collected for each variable given that the instrument is well-calibrated. For example, if the channel width W is measured n times using a well-calibrated optical microscope, the uncertainty σ_W could be taken as one standard deviation of the n measurements.
While the validation process indicates that the experimental method does what it is expected to do, the error propagation tell us how well it does it. For example, one can carry out many inaccurate experiments with high precision and, consequently, report the slip length value with a small standard deviation. While the standard deviation indicates the range in which 68% of all measurements is contained, it does not specify the uncertainty of the experiment. Both the error propagation of the measurements and the standard deviation of the sample should be reported. For example, if the error propagation of a measurement of b is 2% and the standard deviation of a set of measurements of b is 10%, the largest of

the two, the standard deviation, is a good measure of the variation of the experimental conditions (e.g. difference between tested substrates). On the other hand, if the error propagation is 15% and standard deviation of a set of measurements of b is 5%, it is not possible to conclude whether the standard deviation comes from the variation between substrates or from the systematic error propagation of the experimental measurements, neither it is possible to ensure that the presented value of the b is accurate. Therefore, in experiments as delicate as the pressure drop vs flow rate for the estimate of the slip length, both the uncertainty corresponding to the error propagation of the experimental measurements and the standard deviation of the sample must be reported.

6 Correct averaging of the reported DR and b

As mentioned before, the drag reduction factor DR is a function of the characteristic length of the system; i.e. given a specific testing surface, the smaller the system the larger DR (see equations 8 and 9). Therefore, comparing an average value of DR produced by a surface is correct only for systems of the same size. However, given that the height of the channel could slightly differ between experiments, the latter is not easily achievable. On the other hand, the slip length b is independent of the system size and, therefore, reporting an average value is easy. Then, the most appropriate way to report slip length values for a given testing surface is as follows:

1. For each experiment compute b and its experimental uncertainty.
2. Compute the average slip length b_{ave} from all the values of b and report its standard deviation.
3. Using the b_{ave} compute DR for a specific characteristic system length H (this value of H could be the average of all the heights measured across all the experiments, which will be a representative value of the experimental conditions in which the surface was tested).

Finally, in literature b is sometimes computed directly from an average DR. Although doing so will result in relatively similar values when compared with the procedure indicated above, the interpretation of the experimental data is clearly incorrect.

7 Theoretical models and experimental measurements of slip

In this section we present a summary of slip measurements on smooth and structured surfaces and compare them directly with analytical models found in the literature. The results presented here are restricted only to the ones that have been obtained using the pressure drop vs flow rate method. These results are summarised in Table 4, 5 and 6 and Figure 10. In Table 4 it can be seen that the magnitude of the slip length for smooth solvophobic surfaces is highly variable, with several reports of no-slip, and some of the order of tens of nanometers. Results obtained with a number of other high resolution techniques report reproducible slip length values of tens of nanometers for Newtonian liquids flowing on smooth solvophobic surfaces.[1,5] According with Eq. 8, in order to measure nanoscale slip with the pressure drop vs flow rate method, very fine capillaries would be needed to enhance the pressure drop reduction. In addition, given the low flow rate produced in these experiments (normally $< 1\mu L\,min^{-1}$), highly accurate methods are needed to quantify the slip. Choi et al.[57] optimized this method and their slip length measurements are in excellent agreement with values obtained through direct methods.[1,5]
The slip effect is much larger and therefore more easily measured with microfluidic devices on structured, complex surfaces, as shown in Table 5 and 6. Here effective slip length values of the order of several micrometers to tens of micrometers are reported. Structured surfaces can contain pillars, holes, ridges or randomly oriented structures and are classified accordingly (see schematic in Figure 10a and examples found in the literature in Figures 6d-f). In general, the slip length in structured superhydrophobic surfaces can be estimated analytically, and increases with increasing pattern pitch p (the distance between two identical points in adjacent structures) and gas area fraction ϕ_g (for the Cassie state $\phi_g + \phi_s = 1$,

where ϕ_s is the solid fraction). However, this simplified model ignores the effect of the location and curvature of the interface, as discussed in Section 5.6 and in [20,24,37]. For a surface containing pillars with large ϕ_g the effective slip is given by:[13]

$$\frac{b}{p} = \frac{3}{16}\sqrt{\frac{\pi}{1-\phi_g}} - \frac{3\ln\left(1+\sqrt{2}\right)}{2\pi}. \tag{12}$$

For holes:[11]

$$\frac{b}{p} = -A\ln\left(1-\phi_g\right) + B, \tag{13}$$

where A and B are constants defined by the hole geometry and gas fraction. For ridges or grooves oriented parallel to the liquid flow:[10]

$$\frac{b}{p} = \frac{\ln\left[\sec(\pi\phi_g/2)\right]}{\pi}, \tag{14}$$

For ridges oriented perpendicular to the flow slip is half the value given by Equation 14.
Figure 10 summarises the slip results presented in Table 5 for superhydrophobic surfaces containing pillars and holes, ridges and random structures. The slip length is normalized by the pitch of the pattern to allow for the direct comparison with the theoretical predictions. For the case of randomly structured surfaces, the slip length was normalized by the roughness length scale L, which was estimated from micrographs provided in the corresponding article. Although this approach is not completely accurate, it provides a general picture for the results found in the literature by considering the extreme cases and plotting the region in which the results are likely to be found. These plots demonstrate that some experimental slip results agree well with the theoretical predictions. For example, in Figure 10b the results by Ou and Rothstein[58] for $\phi < 0.8$ and the ones from Lee and Kim for $\phi > 0.85$ agree well with the model by Davis and Lauga.[13] However, a large variability in the measured values of slip length for a given gas fraction is presented in all cases. This could be attributed, but not only, to the experimental inaccuracies discussed before, mainly the difficulty in estimating the channel height H in situ, the complexity and challenges of defining an appropriate plane of reference and the adequate monitoring of the fluid temperature. Most of the experimental measurements are larger than the theoretical predictions and the deviation is more drastic for the case of randomly structure surfaces, with exception of the results presented by Song et al.[46], which are in good agreement with the theory by Davis and Lauga (see Figure 10d). As the vertical axis in Figure 10 is in a logarithmic scale, the deviations are larger than they appear to the eye.
Only three pressure drop measurements of slip have been reported so far on liquid-infused surfaces as presented in Table 6 and[26]. In these studies, the viscosity ratio between the working fluid and the infused liquid is a key factor in determining the effective slip provided by these surfaces. Kim and Rothstein[62] showed that pillars and ridges are not effective at retaining the lubricant in place and the partial or complete depletion of lubricant does not permit the quantification of the slip length in these systems. On the contrary, randomly structured surfaces displayed better lubricant retention. Here the large uncertainty on the slip length reported was attributed to the uncertainty of individual measurements and the uncertainty of the channel height. Still clearly further studies are necessary to solidify a picture of reproducible slip effects on structured surfaces.

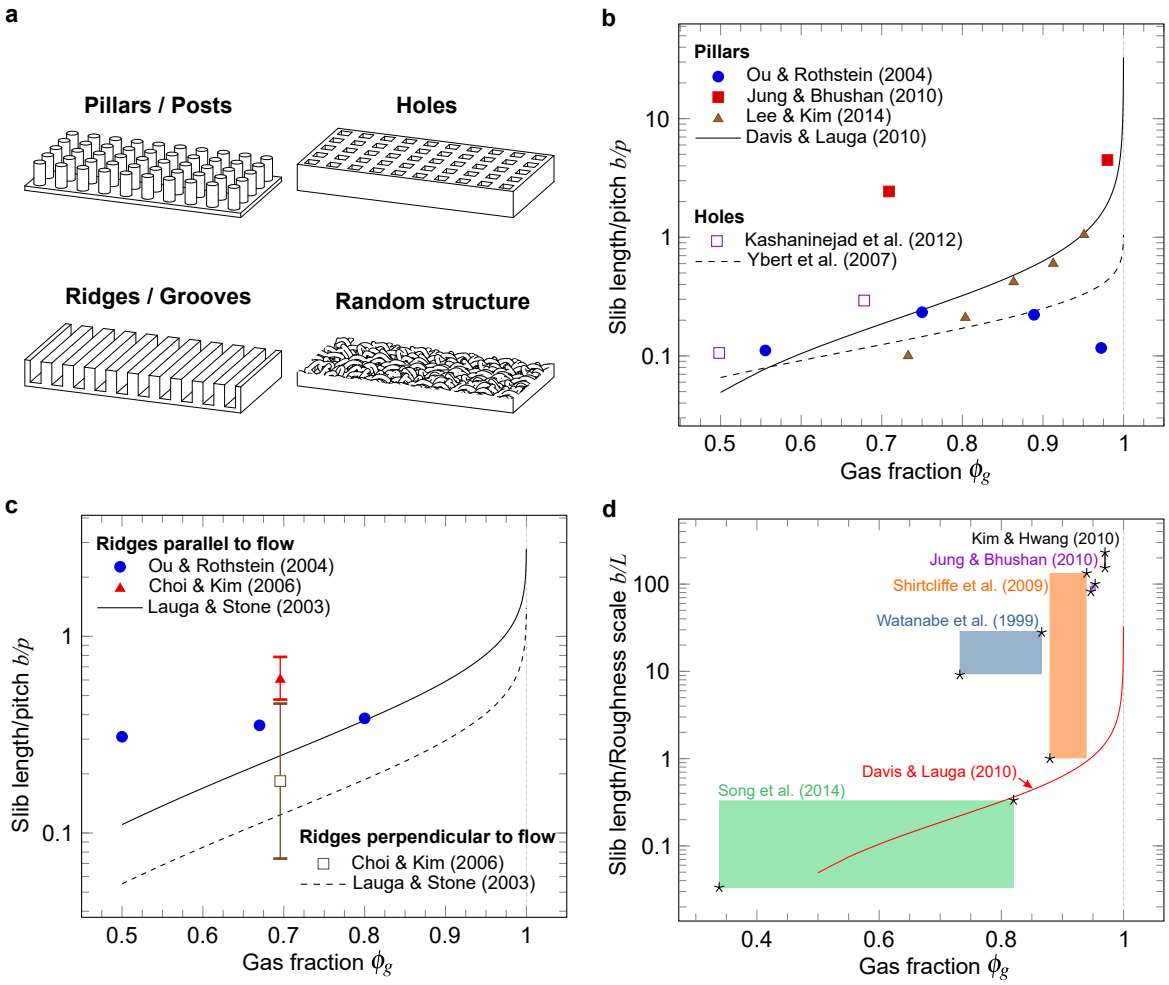

Figure 10: (a) Schematic of structured surfaces used for drag reduction. (b)- (d) Experimental measurements of slip length as a function of the gas fraction ϕ_g obtained by the pressure drop vs flow rate method on surfaces containing (b) pillars/posts and holes, (c) ridges (trenches or grooves), and (d) random structures. The continuous and dashed lines are theoretical predictions according to Eq. 12, 13, and 14, as indicated. When using Eq. 13 for square holes, $A = 0.115$ and $B = -0.014$ as reported by[78]. The shaded regions in part (d) correspond to ranges of slip length values measured in those studies. The vertical axis in all plots is logarithmic, therefore any deviation from the theoretical value is large.

Table 4: Selection of experimental measurements of slip length on smooth surfaces obtained in pressure drop microfluidic measurements

Authors	Testing substrate	Typical roughness	Channel size H or R (µm)	Fluid	Static contact angle	Slip length[2] b (nm)
Schnell (1956) [4]	Pyrex hydrophilic	Not reported	240 - 800	water	Not reported	b_0 (not reported)
	Pyrex + DMDCS[1]	Not reported		water	Not reported	$b_0 + 3 < b < b_0 + 10$ µm
Churaev (1984) [55]	Quartz + TMSCl[1]	Not reported	0.88 - 7.2	water	70° to 90°	30
				mercury	115° to 130°	70
				CCl4	0°	no-slip
				Benzene	0°	no-slip
Mala (1999) [54]	Stainless steel	$R_a = 1.75$µm	50 - 254	water	Not reported	<0
	Fused silica	$R_a = 1.75$µm		water	Not reported	<0
Cheng (2002) [56]	Photoresist	$R_p = 0.5$nm	0.04 to 2.7	water	Not reported	no-slip
				Silicone oil	Not reported	∼18
				Hexane	Not reported	∼9
				Hexadecane	Not reported	∼25-30
				Decane	Not reported	∼14
Choi (2003) [57]	Silicon	$R_{rms} = 11$Å	0.5 and 1	water	∼0°	$-5 < b < 15$
	Silicon + OTS[1]	$R_{rms} = 3.3$ Å		water	∼90°	$5 < b < 35$

[1]DMDCS: dimethyldichlorosilane. TMSCl: trimethylchlorosilane. OTS:octadecyltrichlorosilane.
[2]Only for laminar flow conditions.

Table 5: Selection of experimental measurements of slip length on structured surfaces obtained in pressure drop vs flow rate measurements

Authors	Testing substrate	Type of structures	Typical size of structures[2] (µm)	Channel size H or R (µm)	Fluid	Contact angle θ_{app}	Gas fraction ϕ_g	Slip length[4] b (µm)
Watanabe (1999) [47]	Fluorine alkane + HO silica	Random	h∼10	3000-6000	Tap water	150°	0.73-0.86[7]	91[5] for R=3mm 244[5] for R=6mm
					Glycerin 20 wt%	150°	0.73-0.86[7]	102[5] for R=3mm 265[5] for R=6mm
					Glycerin 30 wt%	150°	0.73-0.86[7]	108[5] for R=3mm 279[5] for R=6mm
Ou (2004) [58]	Silicon + PFDS[1]	Pillars	w=30 45<p<180	76 - 254	Water	130 - 174°	0.56-0.97[7]	5<b<21
		Ridges	w=20 40<p<100				0.5-0.8[7]	12<b<31
Choi (2006) [59]	Silicon oxyde	Ridges	w=0.05 p=0.23 h=0.5	3 - 11	Water	-	0.78	30 ± 16 nm (parallel flow) 0 ± 17 nm (transverse flow)
	Silicon + Teflon	Ridges	w=0.07 p=0.23 h=0.5			145 - 150°	0.70	143 ± 35 nm (parallel flow) 61 ± 44 nm (transverse flow)
Shirtcliffe (2009) [48]	Copper + perfluorocarbon	Ribbons	1x0.1x0.006	438	Water	160°	0.88-0.94[7]	20±14<b<110±23[8]
					Glycerol 50 wt%		0.88-0.94[7]	9±8<b<99±11[8]
Jung (2009) [60]	Epoxy	Flat	-	700	Water	76°	-	<0
	Lotus wax	Flat	-			119°	-	∼24
		Nanotubule	d<0.8			167°	0.95[7]	∼91
		Pillars	d=14 p=23 h=30			160°	0.71	∼56
		Hierarchical	d=14 p=23 h=30			173°	0.98[7]	∼103
		Shark skin	200<w<500 100<s<300			89°	0.16-0.60	∼35
	Acrylic resin	Flat	-	1000	Water	82°	-	<0
		Ribs	w=38 h=90 l=850 s=180			146°	0.86	∼0
Kim (2010) [49]	PTFE	Nanofibers	h=0.5 h/d>20	500	Water	170°	0.97[7]	∼230[5]
Kim (2012) [51]	PDMS	Transverse trenches	15<w<55 s=65 30<h<230	120	Water		0.54-0.81	∼7.5[6]
Kashaninejad (2012) [61]	PDMS	Eccentric holes	6<w<7 p=8.5 h=10	17.9	Water	130 - 135°	0.50-0.68	0.9<b<2.5
Lee (2014) [50]	Silicon + OTS[1]	Pillars	3<d<7 h=6 p=12	30	Water	166°	0.73-0.95	1.2<b<12
Song (2014) [46]	PTFE	Random	7.6<R_{rms}<13.7	137	Water	132 - 150°[3]	0.34-0.80[7]	2<b<20

[1]OTS: Octadecyltrichlorosilane. PFDS: Heptadecafluoro-1,1,2,2-tetrahydrodecyldimethylchlorosilan.
[2]w: width, h: height, d: diameter, p: pitch, s: separation between structures.
[3]Advancing contact angle.
[4]Only for laminar flow conditions.
[5]Estimated from reported drag reduction factor using Eq. 8.
[6]Estimated from reported drag reduction factor using Eq. 9.
[7]Estimated from reported apparent contact angle using $\cos\theta_{app} = (1-\phi_g)\cos\theta - \phi_g$. When θ was unknown, it was assumed to be $90° < \theta < 120°$.
[8]Flow rate dependent.

Table 6: Selection of experimental measurements of effective slip length on liquid-infused structured surfaces obtained in pressure drop microfluidic measurements

Authors	Testing substrate	Type of structures	Typical size of structures[2] (µm)	Channel size H (µm)	Fluid	Lubricant	Viscosity ratio[5]	Static contact angle	Slip length[6] b (µm)
Kim (2016) [62]	PTFE	Random	$10.9<R_{rms}<15.4$	150	Water	Silicone oil (5cP)	0.2	100°[4]	6±7
					Glycerin-water	Silicone oil (5cP)	5.2	100°[4]	7±7
					Glycerin-water	Silicone oil (5cP)	9.2	100°[4]	8±7
	PDMS	Pillars	d=50 h=25		Water and glycerin-water	Silicone oil (5cP) Miglyol oil (10cP)	0.2-9.2 0.1-4.6	Not reported	Lubricant depletion
		Ridges	w=30 30<s<60 h=25		Water and glycerin-water	Silicone oil (5cP) Miglyol oil (10cP)	0.2-9.2 0.1-4.6	Not reported	Lubricant depletion
Lee (2019) [63]	PVA + FDTS[1]	Spherical cavities	h∼100[3]	600	Water[3]	Krytox GPL 103 (80 cSt)	∼0.006	∼107°	∼47[7]

[1]Trichloro(1H,1H,2H,2H-perfluorooctyl) silane.
[2]w: width, h: height, d: diameter, p: pitch, s: separation between structures.
[3]Inferred from figure in the article.
[4]Advancing contact angle.
[5]Estimation based on the dynamic viscosity ratio μ_w/μ_o.
[6]Only for laminar flow conditions.
[7]Estimated from reported drag reduction factor using Eq. 9.

8 Conclusions and outlook

With the emerging manipulation of fluids at very small scales, the need for a better understanding of the interaction between fluids and surfaces has become essential. Correct modelling and fundamental understanding of flow in microfluidic systems rely on the definition of proper wall boundary conditions. The ability to correctly quantify and compare interfacial liquid slip provided by any surface has opened up the prospect of controlling and tuning slip, which is attractive as a passive way to reduce hydrodynamic drag. Many direct and indirect methods are available for the measurement of the slip length b, but the ease of implementation of the pressure drop vs flow rate method makes it highly attractive for many researchers. Here, we have highlighted that, although the method seems simple, there are a wide range of aspects that need consideration for its correct use.

We found that small deviations in the measurement of experimental variables, chiefly fluid temperature (directly linked to the fluid viscosity) and channel dimensions, result in huge errors in the estimation of the slip length. The characteristic length of the system (H for rectangular channels or R for small capillaries) is the most crucial variable affecting the accuracy in the determination of b, with a 5% deviation in the experimental measurement of H resulting in an error of $\sim$ 200% in b for systems in which $H \sim$ 100 µm. Therefore, experiments aimed to report accurate slip length values must be carried out paying attention to factors such as material and dimensions of the device, equipment to impose and measure flow and pressure, liquid temperature, definition of the reference plane, surface cleanliness, sources of errors and contaminant traces.

This review highlights two important aspects; first, the high sensitivity of the slip length measurement with respect to experimental variables and, second, that there exists significant discrepancies between the reported experimental values of b found in the literature and the theoretical models (see Figure 10b-d). This discrepancy is particularly large for the case of randomly structured surfaces. We emphasize that the disagreement between theory and experimental measurements is found to be as large as two orders of magnitude. At this point, it is difficult to point out if the discrepancy comes from sources of systematic experimental error or if it is a real slip effect.

Although the theoretical models presented here are well-accepted and widely used, in general they rely on assumptions that are not always realistic or difficult to attain by experimentalists. For example, the assumption of a pinned flat interface or that the surface texture is completely filled by the lubricant (gas or liquid). Therefore, the ideal nature of some models leaves room for the possibility that the experimental measurements are correct and other mechanisms of slip are being overlooked. However, before addressing that possibility, experimental practices must be reviewed to ensure the accuracy of the method is optimized. Slip length measurements must be accompanied by a proper validation of the experimental setup and a complete estimation of experimental error propagation on the estimation of the slip length value. Only in this way it is possible to determine the accuracy of the measurement and distinguish between the variability of the slip length values coming from the difference between tested surfaces and the one coming from systematic errors of the experiment itself. As an additional remark, we point out that given that the drag reduction factor DR is dependent of the system size, it should not be used as a standard measure to compare the effectiveness of different surfaces in enhancing fluid slip, instead, the slip length b should be used for this purpose.

Outstanding questions remain to be addressed with respect the quantification of slip using the pressure drop vs flow rate method. The proper determination of the channel characteristic dimension is probably the most challenging to address. Ideally, in order to account for any deformation of the channel geometry, the channel dimension should be measured in situ under conditions of flow and only once the channel/device is completely closed. For cases of lubricant-infused structured surfaces (e.g. superhydrophobic and liquid-infused), another two important issues to overcome are: 1) the definition of the experimental plane of reference from which to measure the slip length and 2) the proper characterization of the interface shape. For surfaces containing sufficiently large structures, this could be resolved by integrating additional techniques in conjunction with the pressure drop method, for example laser confocal microscopy. This, however, is difficult to implement in surfaces with nanostructured or randomly patterned topography. New ways to fully describe the lubricant-liquid interface under conditions of flow are necessary to

evaluate the correctness of specific theoretical models and to determine the real configurations of these systems (e.g. solid fraction and curvature and position of the interface). Additionally, as the reduction of the channel dimensions is attractive to enhance the accuracy and resolution of slip measurements, new and simpler methods for measuring accurate flow rates are desirable.
In conclusion, structured surfaces hold promise for passively reducing hydrodynamic drag. Superhydrophobic surfaces face the issue of the plastron stability under conditions of flow or high pressure. Liquid-infused surfaces are more robust against high static pressures, however, are prone to lubricant depletion due to flow-induced shear and, under the currently accepted models, are expected to reduce drag only when the lubricating layer has lower viscosity than the external fluid. For the study of any of these systems, the pressure drop vs flow rate method offers an excellent platform to study the lubricant stability under realistic conditions of flow, which is more rare to achieve with other methods. Finally, although superhydrophobic surfaces have been extensively tested under conditions of flow (Table 5), only three studies have reported slip measurements in liquid-infused surfaces using the pressure drop method (see Table 6 and [26]).

Acknowledgements
CN acknowledges the Australian Research Council for funding (FT180100214). CVS thanks the Costa Rican Ministry of Science and Technology for funding and Tecnologico de Costa Rica for computational resources.

References

[1] C. Neto, D. Evans, E. Bonaccurso, H.-J. Butt, V. Craig, *Rep. Prog. Phys.* **2005**, *68* 32859.

[2] E. Lauga, M. P. Brenner, H. A. Stone, In *Handbook of Experimental Fluid Dynamics*, chapter 15. Springer, New York, **2005**.

[3] D. Tolstoi, *Dokl. Acad. Nauk. SSSR* **1952**, *85* 1329.

[4] E. Schnell, *J. Appl. Phys.* **1956**, *27*, 10 1149.

[5] L. Bocquet, E. Charlaix, *Chem. Soc. Rev.* **2010**, *39*, 3 1073.

[6] T. Lee, E. Charrault, C. Neto, *Adv. Colloid Interface Sci.* **2014**, *210* 21.

[7] S. Peppou-Chapman, J. K. Hong, A. Waterhouse, C. Neto, *Chem. Soc. Rev.* **2020**, *49*, 11 3688.

[8] J. R. Philip, *Z. Angew. Math. Phys.* **1972**, *23*, 3 353.

[9] J. R. Philip, *Z. Angew. Math. Phys.* **1972**, *23*, 6 960.

[10] E. Lauga, H. A. Stone, *J. Fluid Mech.* **2003**, *489* 55.

[11] C. Ybert, C. Barentin, C. Cottin-Bizonne, P. Joseph, L. Bocquet, *Phys. Fluids* **2007**, *19*, 12 123601.

[12] A. M. Davis, E. Lauga, *Phys. Fluids* **2009**, *21*, 1 011701.

[13] A. M. Davis, E. Lauga, *J. Fluid Mech.* **2010**, *661* 402.

[14] C. Schönecker, T. Baier, S. Hardt, *J. Fluid Mech.* **2014**, *740*, 1 168.

[15] C. Schönecker, S. Hardt, *Microfluid. Nanofluid.* **2015**, *19*, 1 199.

[16] R. Sun, C.-O. Ng, *Theor. Comput. Fluid Dyn.* **2017**, *31*, 2 189.

[17] E. Alinovi, A. Bottaro, *Phys. Rev. Fluids* **2018**, *3*, 12 124002.

[18] E. S. Asmolov, T. V. Nizkaya, O. I. Vinogradova, *Phys. Rev. E* **2018**, *98*, 3 033103.

[19] H. Zuo, F. Javadpour, S. Deng, H. Li, *Phys. Fluids* **2020**, *32*, 8 082003.

[20] J. Hyväluoma, J. Harting, *Phys. Rev. Lett.* **2008**, *100*, 24 246001.

[21] J. Hyväluoma, C. Kunert, J. Harting, *J. Phys.: Condens. Matter* **2011**, *23*, 18 184106.

[22] Z. Ge, H. Holmgren, M. Kronbichler, L. Brandt, G. Kreiss, *Phys. Rev. Fluids* **2018**, *3*, 5 1.

[23] J. P. Rothstein, *Annu. Rev. Fluid Mech.* **2010**, *42* 89.

[24] C. Lee, C.-H. Choi, C.-J. Kim, *Exp. Fluids* **2016**, *57*, 12 1.

[25] S. Hardt, G. McHale, *Annu. Rev. Fluid Mech.* **2021**, *54*.

[26] C. Vega-Sánchez, S. Peppou-Chapman, L. Zhu, C. Neto, *Under review* **2021**.

[27] O. I. Vinogradova, *Langmuir* **1995**, *11*, 6 2213.

[28] M. J. Kreder, D. Daniel, A. Tetreault, Z. Cao, B. Lemaire, J. V. Timonen, J. Aizenberg, *Phys. Rev. X* **2018**, *8*, 3 031053.

[29] D. Daniel, J. V. Timonen, R. Li, S. J. Velling, J. Aizenberg, *Nat. Phys.* **2017**, *13*, 10 1020.

[30] J. N. Israelachvili, *Intermolecular and Surface Forces*, Academic Press, **1991**.

[31] J. S. Wexler, A. Grosskopf, M. Chow, Y. Fan, I. Jacobi, H. A. Stone, *Soft Matter* **2015**, *11*, 25 5023.

[32] C. Wang, *Phys. Fluids* **2003**, *15*, 5 1114.

[33] J. S. Wexler, I. Jacobi, H. A. Stone, *Phys. Rev. Lett.* **2015**, *114*, 16 168301.

[34] Y. Zhu, S. Granick, *Phys. Rev. Lett.* **2002**, *88*, 10 106102.

[35] C. Cottin-Bizonne, S. Jurine, J. Baudry, J. Crassous, F. Restagno, E. Charlaix, *Eur. Phys. J. E* **2002**, *9*, 1 47.

[36] R. Gupta, J. Frechette, *Langmuir* **2012**, *28*, 41 14703.

[37] A. Steinberger, C. Cottin-Bizonne, P. Kleimann, E. Charlaix, *Nat. Mater.* **2007**, *6*, 9 665.

[38] L. Zhu, P. Attard, C. Neto, *Langmuir* **2011**, *27*, 11 6712.

[39] L. R. Scarratt, L. Zhu, C. Neto, *Langmuir* **2019**, *35*, 8 2976.

[40] L. R. Scarratt, L. Zhu, C. Neto, *Langmuir* **2020**, *36*, 21 6033.

[41] C.-H. Choi, C.-J. Kim, *Phys. Rev. Lett.* **2006**, *96* 066001.

[42] B. R. Solomon, K. S. Khalil, K. K. Varanasi, *Langmuir* **2014**, *30*, 36 10970.

[43] L. Joly, C. Ybert, L. Bocquet, *Phys. Rev. Lett.* **2006**, *96* 46101.

[44] M. Panahi, R. Jamali, V. F. Rad, M. Khorasani, A. Darudi, A.-R. Moradi, *Sci. Rep.* **2021**, *11*, 1 12916.

[45] R. D. Blevins, *Applied Fluid Dynamics Handbook*, Van Nostrand Reinhold Co., **1984**.

[46] D. Song, R. J. Daniello, J. P. Rothstein, *Exp. Fluids* **2014**, *55*, 8 1.

[47] K. Watanabe, Y. Udagawa, H. Udagawa, *J. Fluid Mech.* **1999**, *381* 225.

[48] N. J. Shirtcliffe, G. McHale, M. I. Newton, Y. Zhang, *ACS Appl. Mater. Interf.* **2009**, *1*, 6 1316.

[49] D. Kim, W. Hwang, *J. Micromech. Microeng.* **2010**, *20*, 2 027002.

[50] A. Lee, H.-Y. Kim, *Phys. Fluids* **2014**, *26*, 7 072002.

[51] T. J. Kim, C. Hidrovo, *Phys. Fluids* **2012**, *24*, 11 112003.

[52] K. Westin, C.-H. Choi, K. Breuer, *Exp. Fluids* **2003**, *34*, 5 635.

[53] L. P. Singh, B. Issenmann, F. Caupin, *Proc. Nat. Acad. Sci.* **2017**, *114*, 17 4312.

[54] G. M. Mala, D. Li, *Int. J. Heat Fluid Flow* **1999**, *20*, 2 142.

[55] N. Churaev, V. Sobolev, A. Somov, *J. Colloid Interf. Sci.* **1984**, *97*, 2 574.

[56] J.-T. Cheng, N. Giordano, *Phys. Rev. E* **2002**, *65*, 3 031206.

[57] C.-H. Choi, K. J. A. Westin, K. S. Breuer, *Phys. Fluids* **2003**, *15*, 10 2897.

[58] J. Ou, B. Perot, J. P. Rothstein, *Phys. Fluids* **2004**, *16*, 12 4635.

[59] C.-H. Choi, U. Ulmanella, J. Kim, C.-M. Ho, C.-J. Kim, *Phys. Fluids* **2006**, *18*, 8 087105.

[60] Y. C. Jung, B. Bhushan, *J. Phys.: Condens. Matter* **2009**, *22*, 3 035104.

[61] N. Kashaninejad, N.-T. Nguyen, W. K. Chan, *Phys. Fluids* **2012**, *24*, 11 112004.

[62] J.-H. Kim, J. P. Rothstein, *Exp. Fluids* **2016**, *57*, 5 81.

[63] S. J. Lee, H. N. Kim, W. Choi, G. Y. Yoon, E. Seo, *Soft Matter* **2019**, *15*, 42 8459.

[64] N.-T. Nguyen, S. T. Wereley, S. A. M. Shaegh, *Fundamentals and Applications of Microfluidics*, Artech house, **2019**.

[65] S. Peppou-Chapman, C. Neto, *Langmuir* **2021**, *37*, 10 3025.

[66] M. A. Samaha, H. Vahedi Tafreshi, M. Gad-el Hak, *Phys. Fluids* **2011**, *23*, 1 012001.

[67] M. A. Samaha, H. V. Tafreshi, M. Gad-el Hak, *Langmuir* **2012**, *28*, 25 9759.

[68] M. A. Samaha, H. Vahedi Tafreshi, M. Gad-el Hak, *Phys. Fluids* **2012**, *24*, 11 112103.

[69] S. Richardson, *J. Fluid Mech.* **1973**, *59*, 4 707.

[70] G. McHale, M. Newton, *J. Appl. Phys.* **2004**, *95*, 1 373.

[71] C. Vega-Sánchez, C. Neto, *Under review* **2021**.

[72] A. S. Haase, J. A. Wood, R. G. Lammertink, J. H. Snoeijer, *Phys. Rev. Fluids* **2016**, *1*, 5 054101.

[73] G. McHale, M. R. Flynn, M. I. Newton, *Soft Matter* **2011**, *7*, 21 10100.

[74] M. Rothenberg, *Phys. Today* **1970**, *23*, 10 17.

[75] H. Christenson, P. Claesson, *Adv. Colloid Interface Sci.* **2001**, *91* 391.

[76] M. James, T. A. Darwish, S. Ciampi, S. O. Sylvester, Z. Zhang, A. Ng, J. J. Gooding, T. L. Hanley, *Soft Matter* **2011**, *7*, 11 5309.

[77] J. Taylor, *Introduction to Error Analysis, the Study of Uncertainties in Physical Measurements*, University Science Books, **1997**.

[78] C.-O. Ng, C. Wang, *Microfluid. Nanofluid.* **2010**, *8*, 3 361.

Chiara Neto received her Masters degree in Chemistry (1998) and PhD (2001) at the University of Florence, Italy. Her PhD work focused on the measurement of hydrodynamic surface forces using the atomic force microscope. After periods of post-doctoral research at the University of Ulm, at Saarland University, and at the Australian National University, since 2007 she works at the University of Sydney. Here she is currently Professor in Physical Chemistry and Australian Research Council Future Fellow, and she leads the Nano-Interfaces research lab. She is one the Founding Directors of the Australasian Colloid and Interface Society.

Christopher Vega received the B.Eng. degree in Electromechanical Engineering from the Costa Rica Institute of Technology (ITCR). In 2011, he was awarded a DAAD scholarship to attend an M.Sc. in Microsystems Engineering at the University of Freiburg, Germany. In 2014, he joined the Department of Electromechanical Engineering at ITCR as a lecturer and researcher, where he worked on the design of low-cost microfluidics and simulations. He is about to complete his PhD degree at the University of Sydney, Australia, working on understanding fluid slip on nanostructured surfaces.

Understanding the fluid slip phenomenon on surfaces is key for manipulating fluids at small scales. However, the correct quantification of fluid slip is experimentally challenging. This article reviews the technical complexity of one of the most widely used techniques, the pressure drop vs. flow rate method, and provides practical solutions to minimize experimental uncertainty in estimating the effective slip length.

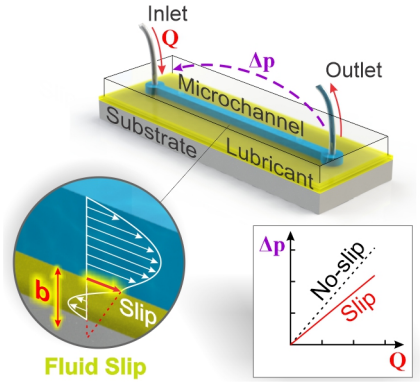

Experimental measurement of fluid slip using the pressure drop vs flow rate method.